Nanoscale

ROYAL SOCIETY OF CHEMISTRY

MINIREVIEW

View Article Online
View Journal | View Issue

Cite this: *Nanoscale*, 2024, **16**, 19589

Luminescent metal nanoclusters and their application in bioimaging

Wenwen Fei, Sheng-Yan Tang and Man-Bo Li *

Received 29th July 2024,
Accepted 17th September 2024

DOI: 10.1039/d4nr03111c

rsc.li/nanoscale

Owing to their unique optical properties and atomically precise structures, metal nanoclusters (MNCs) constitute a new generation of optical probe materials. This mini-review provides a brief overview of luminescence mechanisms and modulation methods of luminescent metal nanoclusters in recent years. Based on these photophysical phenomena, the applications of cluster-based optical probes in optical bioimaging and related sensing, disease diagnosis, and treatment are summarized. Some challenges are also listed at the end.

1. Introduction

Optical microscopic imaging is an optics-based imaging technology that utilizes light's absorption and emission properties to observe and analyze the microscopic world.[1–5] Luminescence-based imaging techniques have been of particular concern because of their sensitivity,[6] selectivity,[7] high contrast,[8] and versatility.[9] Biological imaging is one of the most critical applications.[10] This technique has been used for observing structures of biological tissues[11] and the development of diseases and early diagnosis and treatment.[12] Two types of luminescence exist in biological tissues. The first is the luminescence of substances inherent in the tissue, such as mitochondrial natriuretic hormone (NADH), chlorophyll, and other luminescent substances, and the second is the artificial addition of luminescent probes to make the tissue luminescent in the imaging method. Standard optical imaging probes are composed of a targeting moiety and fluorochromes.[13] When excited at a specific wavelength, probe molecules emit light, revealing specific structures or sites within a biological tissue. This enables the researcher to make precise and corresponding observations. There have been many years of research on optical imaging probes, roughly divided into three stages.

Organic chromophores with large conjugated systems were initially utilized as the primary generation of optical probes.[14–16] Since the discovery of the first organic fluorophore, quinoline, in 1834, organic dyes have been the dominant category of materials in optical probes because of their high degree of customization.[17] According to the strategies of modern organic chemistry, photophysical parameters such as excitation and emission spectra,[18] molar absorption coefficients,[19] Stokes shifts,[20] and quantum yields[21] of organic small molecules can be accurately tailored to the imaging requirements.[22–27] Nevertheless, popular organic small-mole-

Institutes of Physical Science and Information Technology, Key Laboratory of Structure and Functional Regulation of Hybrid Materials of Ministry of Education, Anhui University, Hefei, 230601, China. E-mail: mbli@ahu.edu.cn

Wenwen Fei

Wenwen Fei received her Ph.D degree in physical chemistry from the University of Padua (Italy) in 2020 under the supervision of Prof. Flavio Maran. She is currently a lecturer at Anhui University, and her research focuses on photo-functional ligand-protected coinage metal nanoclusters.

Sheng-Yan Tang

Sheng-Yan Tang is currently a master's student at the Institutes of Physical Science and Information Technology of Anhui University. Her research interest focuses on the synthesis and catalytic properties of pincer ligand-protected metal nanoclusters.

cule fluorophores (*e.g.*, rhodamine 6G and fluorescein) have been documented to be toxic at moderate concentrations.[28] This has substantially restricted the practical application of organic small-molecule optical probes in biological imaging. Subsequently, there were certainly a number of other fluorescent probes such as metal complexes that emerged. They can be used to enhance the photostability of organic small-molecule dyes to some extent.[29,30]

The resolution of microimaging techniques related to bioimaging has improved dramatically over the past 20 years, with some already achieving the nanometer scale. Several luminescent nanoparticles have emerged as second-generation optical probe materials in this context.[31] Most of the nanoparticles used in bioimaging or biosensing are inert and non-toxic or can be rendered non-toxic by surface modification.[32,33] Besides that, the retention time of nanoparticles *in vivo* is much longer than that of small-molecule fluorophores, making it possible to visualize them for a prolonged time.[34] Meanwhile, nanoparticles can organically integrate imaging, diagnostics, and therapy into a single platform. Thus, fluorophores, targeting moieties and drug molecules, can be embedded on the surface of nanoparticles, allowing for simultaneous detection and treatment.[35–38] In the actual implementation process, nanoparticles nevertheless progressively display some disadvantages. For example, some tumors possess high permeability and retention effects, and the constriction of blood vessels would cause aggregation of nanoparticles.[39] Moreover, kidneys do not efficiently eliminate larger-size nanoparticles.[40,41]

Atomically precise metal nanoclusters (MNCs) are emerging nanomaterials with dimensions between 1 and 3 nm.[42–45] They are considered a bridge between plasmonic metal nanoparticles and small molecules with excellent biocompatibility[46,47] and favorable photostability.[48] Their conduction band undergoes a distinct quantization effect, leading to unique optical properties.[49–52] Meanwhile, the optical properties of metal nanoclusters can be precisely modulated with atomic precision.[53] Being molecular-like and ultrasmall-sized, metal nanoclusters can be efficiently cleared by the kidneys and characterized by intrinsic near-infrared region luminescence.[54,55] Luminescent metal nanoclusters perfectly compensate for the drawbacks of organic small molecules and nanoparticles, demonstrating the prospect of enhanced clinical application.[56,57] Over the past few decades, there has been considerable advancement in exploring synthetic methods,[58–60] structural evolution,[61,62] and related properties of MNCs. The investigation of their optical properties, luminescence mechanisms, and biological applications[63–67] has indicated that metal nanoclusters can be excellent optical probes. Not only water-soluble, but also liposoluble MNCs have been chosen for research in the field of optical bioimaging.[68,69] In recent years, the emergence of cluster aggregation-induced emission enhancement,[70] post-functionalization,[71] and other strategies has laid the foundation for atomically precise metal nanoclusters as third-generation optical probes (Scheme 1).

This mini-review briefly provides an overview of the research progress of MNCs that has been conducted using optical imaging probes in the following four aspects: (1) diverse photophysical characteristics; (2) structural and photoluminescence modulation; (3) application in optical bioimaging; and (4) current challenges.

Man-Bo Li

Man-Bo Li was born in Hubei, China, in 1986. He received his B.S. (2008) and Ph.D (2013) degrees from the University of Science and Technology of China (USTC). After postdoctoral research at the Chinese Academy of Sciences (CAS), King Abdullah University of Science and Technology (KAUST) and Stockholm University (SU), he started his independent academic career as a professor at Anhui University in 2019. Professor Li has authored over 60 scientific publications and has received scientific awards, including the Thieme Chemistry Journals Award. His current research interests focus on the synthesis and catalysis of atomically precise metal nanoclusters.

2. Photoluminescence activity

MNCs exhibit distinct highest occupied molecular orbital (HOMO)–lowest unoccupied molecular orbital (LUMO) transitions accompanied by size-sensitive physicochemical properties.[72,73] Early reports indicated that the scale-dependent luminescence of these molecular-like clusters mainly originated from the intraband transitions of free electrons[74] (Fig. 1). Clarifying MNCs' luminescence mechanisms and various luminescence behaviors is essential for exploring new optical probes. At the beginning of the research on luminescent metal nanoclusters, the role of ligands was not emphasized. However, in the last twenty years, with an in-depth understanding of luminescent MNCs' electronic and geometric structures, the contribution of ligands to the photophysical behaviors of metal nanoclusters has been increasingly acknowledged.[75] Ligand-to-metal (LMCT) and/or ligand-to-metal–metal charge transfer (LMMCT) have been recognized as primarily responsible for MNCs' photoluminescence properties. Jin *et al.* proposed two photoluminescence mechanisms for a thiol-protected gold nanocluster $Au_{25}(SR)_{18}$ (SR = thiolate): the LMCT process *via* "Au–S" bonds and the direct electron transfer from electron-rich atoms or groups to the metal kernel.[76] The strength of interactions between the coordinating atoms and the metals may also affect the photoluminescence intensity of the clusters to a certain extent. For instance, the weak interaction between Se and Au results in a relatively weaker emission of $Au_{25}(SeR)_{18}$ (SeR = selenium) compared to the $Au_{25}(SR)_{18}$ nanocluster.[77]

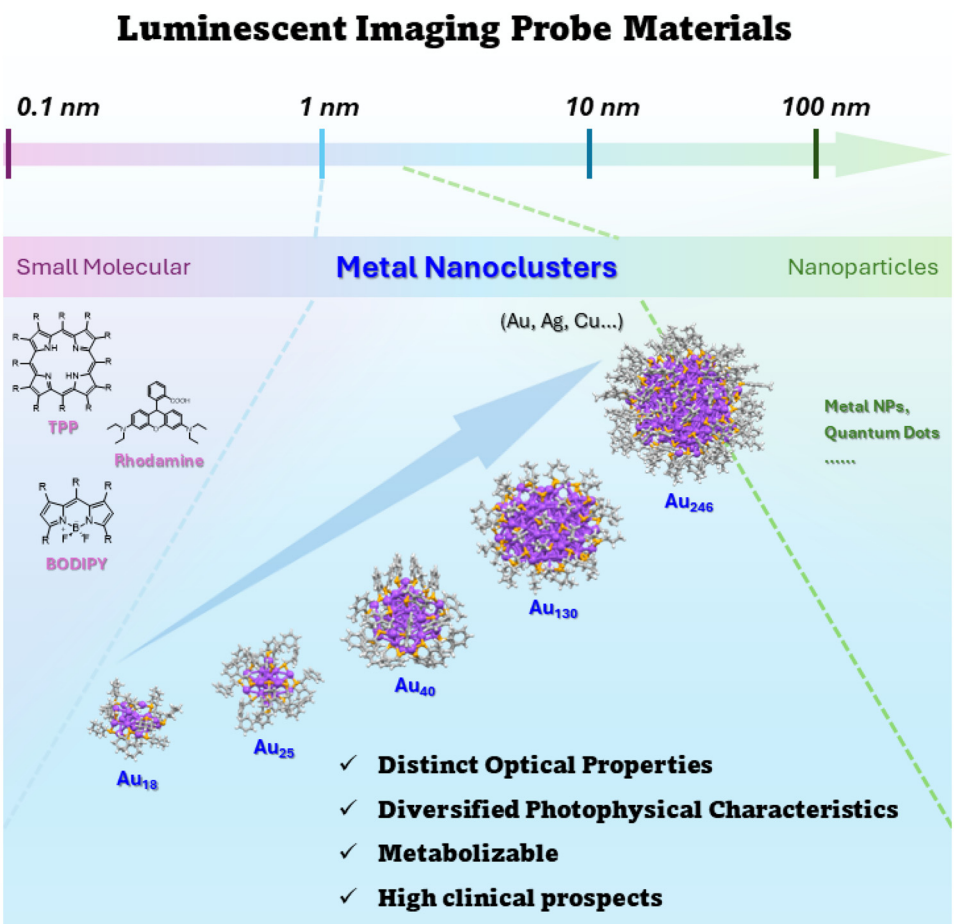

Scheme 1 Three kinds of optical probe materials with size increased.

2.1. Dual emission

Dual-emission optical probes typically display two distinguishable emission peaks, usually separated by intervals of tens of nanometers.[78–81] The distinct emission positions are frequently subject to external circumstances, such as the interaction of the probe with the target molecule or tissue.[82,83] In contrast to conventional optical probes with a single emission peak, a dual-emission optical probe can convey two simultaneous kinds of messages. Therefore, it will have broader applications in chemical analysis and life-based information transfer.[84,85] Owing to the abundant energy level composition of MNCs, two types of electronic transitions are likely to be generated under one excitation condition. Therefore, the prospect of their application in the field of dual emission is extremely promising.[86] Chen *et al.* discovered double emission in non-homogeneously sized copper nanoclusters in 2011[87] (Fig. 2a–c). In 2020, Jin *et al.* observed photo-induced structural distortions accompanied by electron redistribution during excited state processes in a series of gold nanoclusters, $Au_{24}(STBBM)_{20}$, $Au_{14}Cd(SAdm)_{12}$, and $Au_{24}(PET)_{20}$ (STBBM = 4-*tert*-butylphenylmethancan, SAdm = 1-adamantanethiol, and PET = 2-phenylethanethiol), in which photo-induced structural distortions of clusters accompanied by electron redistribution in the excited state were found. This process leads to clusters with extended photoluminescence lifetimes and dual emission in the near-infrared region, which exhibit a highly sensitive response to solvent polarity, viscosity, and temperature[88] (Fig. 2d–i). Then, Jin *et al.* reported the synthesis of $Au_{42}(PET)_{32}$ nanoclusters in 2022. They were surprised that this cluster exhibited dual-emission phenomena at 875 and 1040 nm, attributed to fluorescence and phosphorescence, respectively. It has a quantum yield of 11.9% in solvent at room temperature, which is very rare among thiol-protected gold nanoclusters.[89] Enhancing the intersystem crossing efficiency from singlet to triplet excited states induced by dipole interactions between molecules could suppress the fluorescence and enhance the phosphorescence concurrently.[90] Lately, several DNA-protected metal nanoclusters with dual emissions have emerged in abundance. Some transient absorption dynamics and density functional theory (DFT) also provide theoretical evidence.[91–95]

2.2. Aggregation-induced emission (AIE)

The aggregation-induced emission (AIE) phenomenon, discovered by Tang *et al.* in 2001,[96] was also found in metal nanoclusters. Restriction of intramolecular motion (RIM) is con-

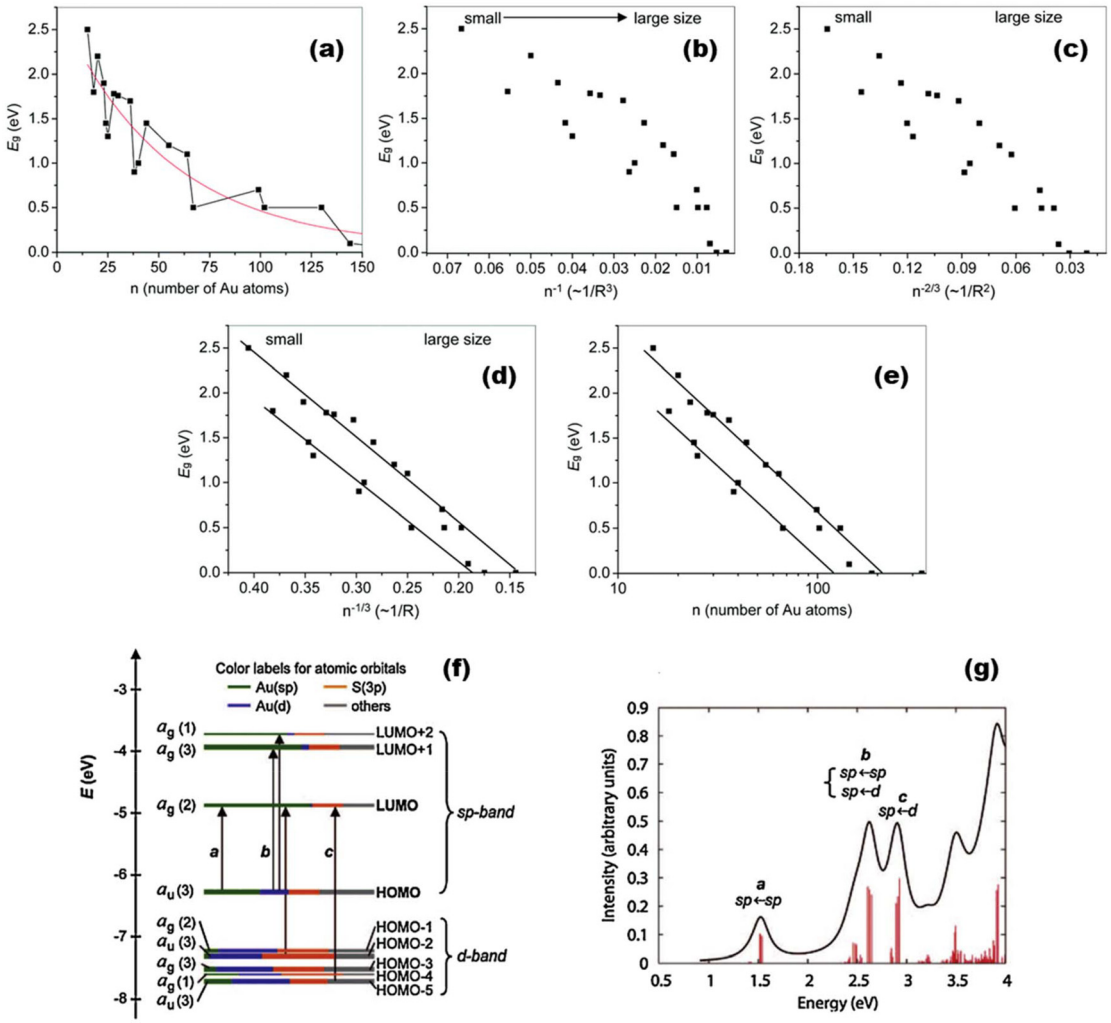

Fig. 1 (a) Trends of bandgap E_g energies with the size of thiolate-protected nanoclusters (the lines serve as guides to the eye); (b) E_g against 1/n; (c) E_g against $n^{-2/3}$; (d) E_g against $n^{-1/3}$; and (e) E_g against log(n). The lines in (d) and (e) are linear regressions with $n^{-1/3}$ and log(n), respectively. Note: R in the horizontal coordinate represents the carbon tailor of thiolate. Reproduced from ref. 72 with permission from the Royal Society of Chemistry, copyright (2014); (f) Kohn–Sham orbital energy level diagram for a model compound $Au_{25}(SH)_{18}^-$. Note: Au_{6sp} = green, Au_{5d} = blue, S_{3p} = orange, and others = gray. (g) The theoretical absorption spectrum of $Au_{25}(SH)_{18}^-$. Peak assignments: peak a = 1.8 eV, peak b = 2.75 eV, and peak c = 3.1 eV. Reproduced from ref. 73 with permission from the American Chemical Society, copyright (2008).

sidered to be the core of the AIE mechanism.[97] The AIE behavior of metal nanoclusters can display longer decay lifetimes (μs-level), redder emissions, and larger Stokes shifts. Consequently, metal nanoclusters can break through the limitations of traditional materials as novel optical probes for AIE.[98] Conventional AIE luminogens generally have a propeller-like steric conformation, based on which Zhang *et al.* prepared a pair of chiral trinuclear Cu(I) clusters (*R*/*S*-Cu_3). They have achieved an AIE factor of 17.3. The luminescence mechanism was shown to be metal cluster-centered (MCC) and triplet metal-to-ligand charge transfer (^{3}MLCT) processes[99] (Fig. 3). Xie's group recently demonstrated the AIE of nanoclusters, which provides a new path toward creating unique photoluminescent materials. An Au(0)@Au(I)–thiolate core–shell-type structure is considered in Au nanoclusters, where surface Au–thiolate complexes are the primary sources of AIE characteristics.[100,101] Bain *et al.* have identified AIE from an Ag (I)–thiolate complex on the MNCs' surface, which is generated from metal-centered triplet states.[102] The role of surface motifs is also manifested in other doped MNCs.[103,104] Furthermore, the emission intensity of AIE is largely dictated by the aggregation degree of NCs.[105–107] Due to the complexity of the cluster structure, new modes of AIE emission mechanisms, such as "dissociation–aggregation" and "the restriction of intramolecular rotation", have been derived.[108–110]

2.3. Thermally activated delayed fluorescence (TADF)

Thermally activated delayed fluorescent (TADF) materials can achieve almost 100% internal quantum efficiency by a reversible intersystem crossing process from the lowest triplet

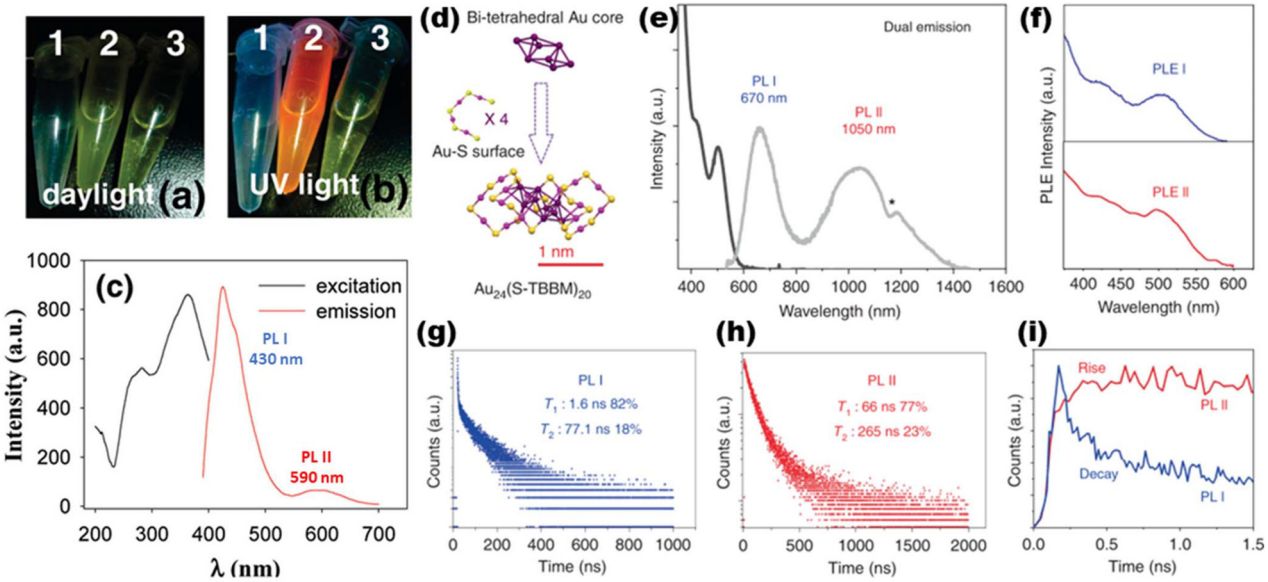

Fig. 2 Photographs of samples under (a) daylight and (b) UV light: (1) empty; (2) nanoclusters; and (3) ligands. (c) Excitation (black) and emission (red) spectra of the copper nanoclusters (solvent: $CHCl_3$) (ref. 87). (d) Precise structure of the Au_{24} nanoclusters. Note: Au = purple/magenta; S = yellow; others are omitted for clarity. (e) UV-vis (black) and PL (gray) spectra of Au_{24}. (f) Excitation spectra of the two emissions. Time-correlated single-photon counting (TCSPC) spectra of PL I (g) and PL II (h). (i) Comparison of the TCSPC spectra of PL I and PL II in the initial 1.5 ns. Reproduced from ref. 88 with permission from Springer Nature, copyright (2020).

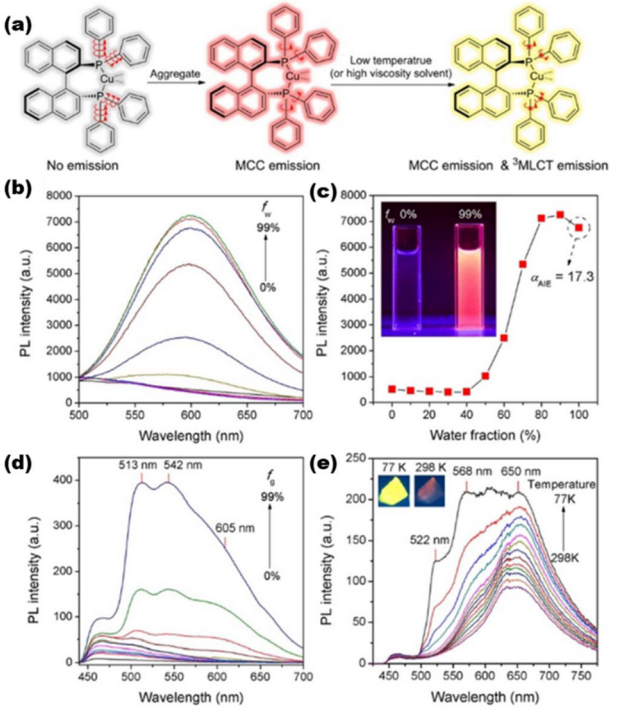

Fig. 3 (a) RIM mechanism of the *R*/*S*-Cu_3 nanocluster; (b) emission spectra of *R*/*S*-Cu_3 in DMSO–H_2O mixtures with different ratios; (c) emission intensity of *R*/*S*-Cu_3 at 605 nm as a function of the volume fraction of water (f_w); (d) emission spectra of *R*/*S*-Cu_3 in EtOH–glycerol mixtures with different f_g values; and (e) temperature-dependent emission spectra of *R*/*S*-Cu_3 in the solid state. Reproduced from ref. 99 with permission from Wiley, copyright (2020).

excited state to the lowest singlet excited state.[111–113] TADF optical probes are significant in long-life imaging, temperature or oxygen sensing, and photodynamic therapy. While investigating four structurally identical Ag_{22} clusters, Sun *et al.* realized that for such eight-electron superatomic silver nanoclusters, different interfacial bonding structures resulted in a unique donor–acceptor type of electronic structure, which further triggered the TADF properties of the nanoclusters[114] (Fig. 4). Zheng *et al.* have recently reported the largest Au–Ag-oxo bimetallic nanocluster to date, $Au_{18}Ag_{26}(R_1COO)_{12}(R_2C{\equiv}C)_{24}(\mu_4\text{-}O)_2(\mu_3\text{-}O)_2$ (R_1 = CH_3–, Ph–, CHOPh– or CF_3Ph–; R_2 = Ph– or FPh–). Single-crystal X-ray diffraction reveals strong π···π and CH···π interactions and metal–oxygen–metal interactions generated by the centrally coordinated O^{2-}. These make such nanoclusters exhibit excellent TADF properties. These include a very small S_1–T_1 energy gap (55.5 meV), a high absolute quantum yield (86.7%), and an ultra-long TADF decay time (1.6 μs).[115]

2.4. Förster/fluorescence resonance energy transfer (FRET)

The theoretical physicist Theodor Förster proposed equations in 1948 for the efficiency of electron excitation transfer from an energy donor to an acceptor.[116–118] Thus, Förster/fluorescence resonance energy transfer (FRET) is a non-radiative energy transfer process *via* long-range dipole–dipole interactions from a donor to an acceptor. The advantages of FRET-based fluorescent probes include significant Stokes shifts,[119] ratiometric sensing, and dual/multi-analyte response systems. They have powerful potential applications in detecting or imaging cations, anions, neutral small molecules, bio-

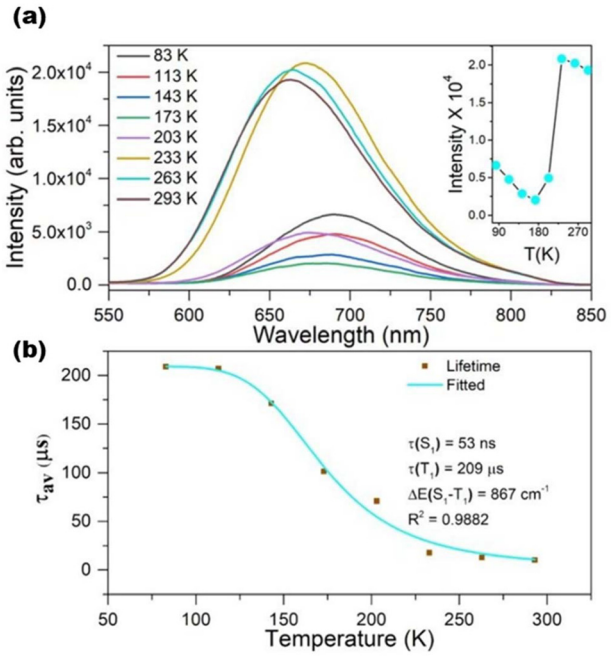

Fig. 4 (a) Temperature-dependent emission spectra of Ag_{22} nanoclusters at 365 nm excitation. Inset: temperature-dependent solid-state photoluminescence intensity from 83 to 293 K. (b) Plot of photoluminescence lifetime at 670 nm against temperature for Ag_{22} and the data fitting. Reproduced from ref. 114 with permission from Wiley, copyright (2022).

molecules, cellular microenvironments, and dual/multi-analyte response systems.[120,121] Understanding the FRET process of metal nanoparticles at the atomic level has long been challenging due to the lack of precise systems with defined molecular distances and orientations. Recently, the FRET behavior of MNCs has been reported for the first time from a theoretical and experimental point of view by Häkkinen and Pettersson *et al.* Azadioxotriangulenium dye (KU) acts as an electron donor and $Au_{25}(p\text{-MBA})_{18}$ (p-MBA = *para*-mercaptobenzoic acid) acts as an electron acceptor. They found that KU can bind to the cluster surface (at a distance of 0.2 nm) by interacting with the ligand on the cluster surface as a monomer, thus triggering the FRET behavior of the cluster[122] (Fig. 5). Later, Zhu *et al.* cleverly achieved FRET between two atomically precise Cu nanoclusters *via* co-crystallization-induced spatial confinement. They chose $Cu_{10}(p\text{-MBT})_{10}(PPh_3)_4$ as the electron donor and $Cu_8(p\text{-MBT})_8(PPh_3)_4$ as the electron acceptor and accurately controlled the distances between the two utilizing co-crystallization. DFT was adopted to gain a deeper understanding of the role of distance and dipole orientation of the molecules to account for the FRET process between two cluster molecules at the electronic structure level.[123]

2.5. Nonlinear optical behaviors

Multiphoton fluorescent probes, which have flourished in the last decade, incorporate powerful laser technological advantages and have played a significant role in bioimaging in recent years.[124–126] Due to the high-order nonlinear relation-

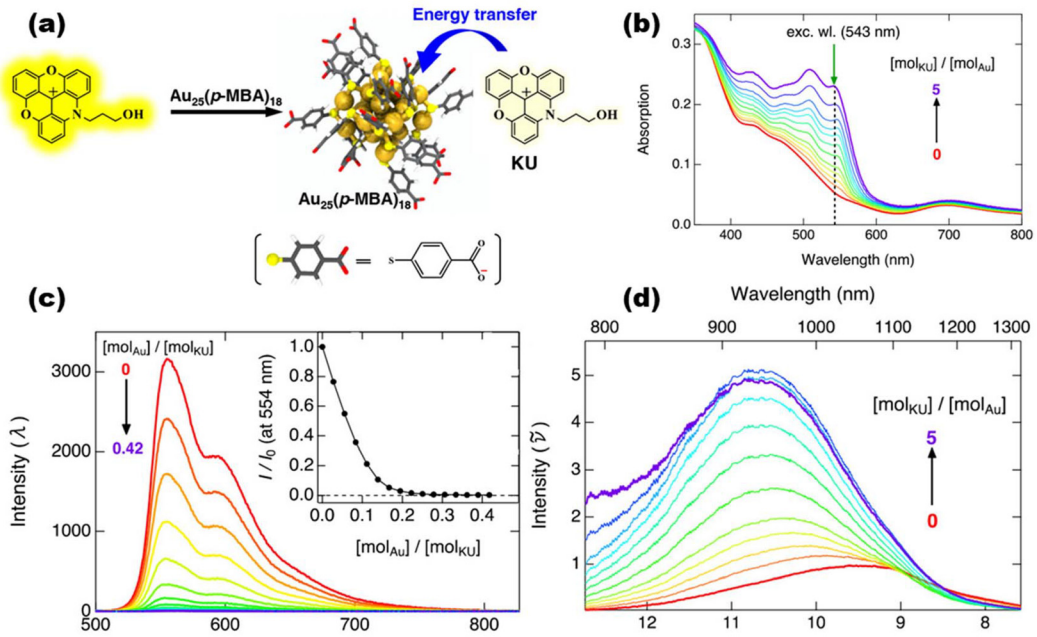

Fig. 5 (a) Schematic illustration depicting how the KU dye and $Au_{25}(p\text{-MBA})_{18}$ nanocluster interact and transfer energy. (b) Emission spectra of KU at pH = 10 for various $Au_{25}(p\text{-MBA})_{18}$ molar ratios. The relative intensity at 554 nm is shown against the molar ratio of $[mol_{Au}]/[mol_{KU}]$ in the inset. (c) UV-vis spectra of $Au_{25}(p\text{-MBA})_{18}$ (c = 5.8 μM) with the addition of KU. (d) Corresponding emission spectra in wavenumbers at an excitation wavelength of 543 nm, as illustrated by the green arrow in (b). Reproduced from ref. 122 with permission from the American Chemical Society, copyright (2020).

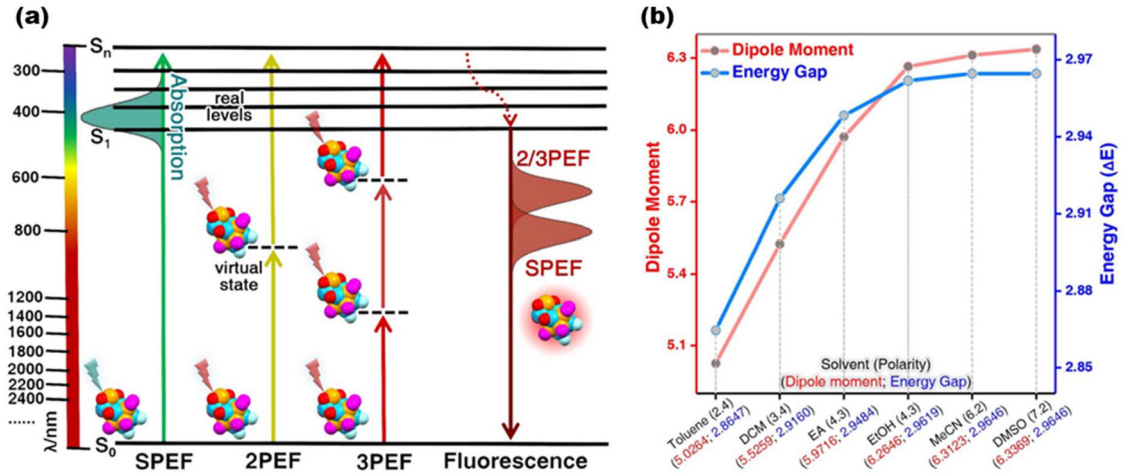

Fig. 6 (a) Schematic illustration of single/two/three-photon excited fluorescence processes; (b) proportionality between solvent polarity and the simulated dipole moment/HOMO–LUMO energy gap of nanoclusters. Reproduced from ref. 131 with permission from Wiley, copyright (2022).

ship between multiphoton emission and the power of excitation light, the emission light is confined to the neighborhood of the focal point, thus providing an ultra-high signal-to-background ratio.[127] Also, its excitation wavelength in the near-infrared region results in less scattering of the excitation light by biological tissues.[128] Goodson III and his collaborators have been working on the multiphoton luminescence properties of metal nanoclusters since as early as 2008. By then, they had noted the high potential of MNCs in this area.[129,130] Zhu and co-workers first reported that solvent modulation of the excited state dipole moments of cluster molecules increases the clusters' nonlinear effect, and their multiphoton emission properties have also been investigated[131] (Fig. 6). Moreover, detailed studies originating from UV-vis absorption spectroscopy[132] have determined the high tunability of the clusters concerning their third-order nonlinear optical properties such as two-photon absorption coefficients, optical limiting thresholds, nonlinear refractive indices, and third-order nonlinear optical magnetization.[133–135] On the other hand, the second harmonic generation (SHG), which also belongs to the nonlinear effect, is a new technology that has emerged recently. Compared with multiphoton luminescence, the SHG emission range is narrower, which gives the SGH probes the advantages of no signal saturation and fluorescence bleaching.[136] Since the SHG effect has a more stringent requirement in the molecular stacking mode, there have only been some sporadic reports on clusters until now.[137]

Besides the above mentioned interesting photophysical properties and the corresponding probe modes, MNCs have substantially shown long afterglow emission, circularly polarized luminescence, *etc*.[138–141]

3. Photoluminescence regulation

Compared with other conventional luminescent materials, such as organic fluorescent dyes and quantum dots, the luminescence efficiency (*e.g.*, quantum yield) of MNCs is relatively low. Still, their ability to absorb light (*e.g.*, extinction coefficient) is at a very high level compared with various optical materials. Therefore, optimizing the emissive ability of MNCs and clarifying the luminescence mechanism of the clusters are of great importance for their utilization as a high-performance category of optical probes. Until now, numerous efforts have been made to maximize the intensity and biotissue-friendly emission in the red region.

Ligand exchange and metal doping are two of the most important and fundamental ways to modulate the optical properties of metal nanoclusters.[142–151] Zhu *et al.* accurately increased the QY of the clusters and achieved a redshift of the emission peak by altering the electron-induced effect on the ligands of the Au_2Cu_6 nanocluster.[152] They also successfully achieved the simultaneous enhancement of PL and CPL intensities by increasing the alloying degree and chiral ligand induction from the racemic template $Au_{14}Cd$ nanocluster using both ligand exchange and metal doping.[153] Compared to other chiral luminescent materials, chiral nanoclusters have diverse and atomically precise structures. Sun *et al.* utilized different concentrations of *R*/*S*-BNP (BNP = *R*/*S*-1,1′-binaphthyl-2,2′-diyl hydrogen phosphate) to transform otherwise symmetric metal clusters into two chiral Ag_{16} and Ag_{29} nanoclusters.[154] Bakr *et al.* synthesized functional Au_2Cu_2(*R*/*S*-BTT)$_4$ nanoclusters with AIE enhancement using a chiral ligand *R*/*S*-BTT (enantiopure *R*/*S*-4-benzylthiazolidine-2-thione). An efficiency leap (36.5%) in the cluster-based CP-LED materials was achieved[155] (Fig. 7a). More recently, Jin *et al.* reconsidered the Au_{25} and Ag_{25} nanoclusters (the same structural characterization methods, ligands are omitted). They found that the faint photoluminescence of Au_{25} in the near-infrared region is due to the strong electron-vibration coupling inside the cluster, and therefore, single-atom doping of Au_{25} can effectively enhance the coupling of the exciton with staple

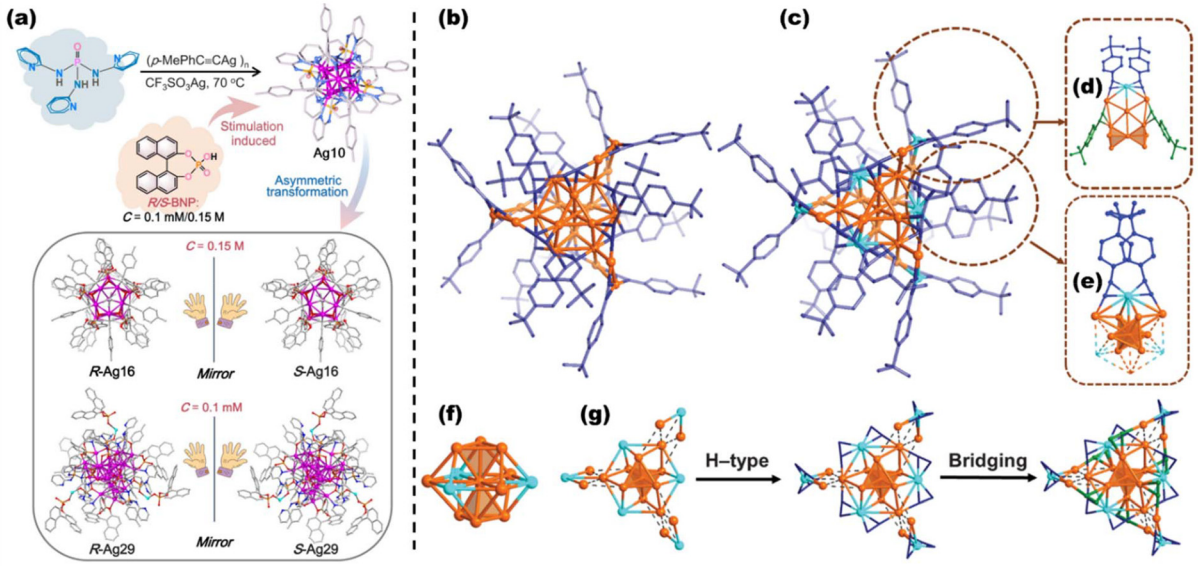

Fig. 7 (a) Varying amounts of *R*/*S*-BNP ligands bring about the asymmetric transformation of achiral Ag_{10} to chiral *R*/*S*-Ag_{16} and *R*/*S*-Ag_{29}. Reproduced from ref. 155 with permission from the American Chemical Society, copyright (2024). Topological structures of Au_{22} (b) and $Au_{16}Cu_6$ (c) nanoclusters, H atoms are omitted for clarity. Coordination modes of Cu atoms in the Au_2Cu motifs (d) and Au_6Cu_6 motifs of $Au_{16}Cu_6$. (f) $Au_{10}Cu_3$ kernel of $Au_{16}Cu_6$. (g) Structural evolution of $Au_{16}Cu_6$, *tert*-butyl phenyl groups are omitted for clarity. Note: Au = orange; Cu = light blue; C = blue/deep blue/or green. Reproduced from ref. 164 with permission from the American Association for the Advancement of Science, copyright (2024).

vibrations but reduces the coupling with the core breathing and quadrupolar modes. They revealed a linear pattern in the photoluminescence lifetimes of the three $Au_{24}Hg$, Au_{25}, and $Au_{24}Cd$ species, implying that doping produces a mechanism to suppress nonradiative decay in the modulation of cluster photoluminescence enhancement. In the study of Ag_{25}, they instead identified that the doping of gold atoms triggers them to produce stronger electronic vibrational coupling, counteracting the radiative enhancement effect. Therefore Au_xAg_{25-x} shows a lower quantum yield.[156] Pniakowska *et al.* demonstrated that doping also promotes nonlinear photoluminescence.[157] Meanwhile, the transition from metallic to nonmetallic behavior, the impact of solvents and metal dopants on electron dynamics, valence electron-dependent relaxation pathways, *etc*. have been explained by some model systems. The critical role of metal atoms and ligands also has a significant effect on ultrafast relaxation processes.[158–163]

In an attempt to resolve the long-standing dilemma that the quantum yield of room-temperature photoluminescence of nanoclusters in solution has been relatively low, Wang *et al.* investigated $Au_{22}(^t$BuPhC≡C$)_{18}$(Au_{22} for short) and its heterometallic doped $Au_{16}Cu_6(^t$BuPhC≡C$)_{18}$($Au_{16}Cu_6$ for short). It was discovered that Cu doping significantly suppresses the nonradiative decay of the nanoclusters (*ca.* 60-fold) (^{t}Bu = *tert*-butyl and Ph = phenyl) and efficiently facilitates the intersystem crossing rate (*ca.* 300-fold). $Au_{16}Cu_6$ exhibits a room-temperature photoluminescence quantum yield close to 100% in the NIR region in a deaerated solution. A high quantum yield of 61% is also achievable even in an oxygen-saturated solution[164] (Fig. 7b). Provided that metal doping belongs to the endogenous regulation method, ligand modifications will show an exogenous manner. Jin *et al.* observed that the QY of the $Au_{52}(SR)_{32}$ nanocluster protected by a series of different aromatic thiols was lower with smaller *para*-position substituents. It was found that the large enhancement of the QY with fewer methyl groups on the ligands implies nonradiative decay *via* the multiphonon process mediated by C–H bonds. Single-crystal X-ray diffraction suggests that smaller substituents lead to stronger π···π interactions between the ligands stacking on the Au_{52} kernel, thus limiting the vibration and rotation of the ligands.[165]

In addition to these basic techniques,[166] many other methods for regulating the optical properties of clusters have been proposed in recent years, such as molecular self-assembly, loading materials, post-modification, *etc*. The optical properties of clusters are progressively developed in the direction of diversification and functionalization. Zang *et al.* have selected a classical anionic nanocluster $[Ag_{29}(BDT)_{12}(TPP)_4]^{3-}$ (BDT = 1,3-benzenedithiol and TPP = tripenylphosphine) and a conventional photosensitizer, $Ru(bpy)_3^{2+}$ (bpy = 2,2′-bipyridine), and employed electrostatic interactions and intramolecular hydrogen bonding to produce the co-assembly effect. Single-crystal X-ray diffraction showed that $Ru(bpy)_3^{2+}$ was confined in the lattice vacancies of Ag_{29}, reducing the symmetry of the pristine structure of Ag_{29}. As a result of this enhanced asymmetry, this self-assembled $Ag_{29}Ru$ arising from the utilization of supramolecular interactions exhibits typical two-photon excitation photoluminescence.[167] The emission efficiency of a single MNC indeed hampers its practical application, and conventional ligand engineering approaches have so far lacked the means to solve this issue completely. Shen *et al.* proposed a DNA framework-guided strategy for preparing

highly luminescent metal nanoclusters. They used an amphiphilic DNA framework consisting of a hydrophobic alkyl core and a rigid DNA framework shell to act as a nucleation site and provide well-defined confinement for the self-limiting aggregation of the nanoclusters (Fig. 8a). This approach produced homogeneous cluster nano-aggregates (10.1 ± 1.2 nm) with excellent nanoscale precision. Remarkably, the strategy is shown to apply to a wide range of clusters (Fig. 8b), leading to a substantial increase in the emission and quantum yields up to 3011-fold and 87-fold, respectively.[168] Some water-soluble polymers can also serve as ideal assembly carriers for nanoclusters, which have been demonstrated to promote cluster relaxation in the excited state and inhibit non-radiative transitions while enhancing the biocompatibility of the clusters.[169] Wu *et al.* used $Au_{10}(SR)_6$ as a template and then cascaded $Au_{10}(SR)_6$ with 6-azido-2-thiothymidine (ATT), L-arginine (ARG), and tetra-*n*-octylammonium bromide (TOA) as the three-layer surface ligands, respectively. Among them, ATT and ARG can be anchored by the hydrogen bond formed between the two ligands, while ARG and TOA can be connected by electrostatic interactions between the carboxyl groups and the *meso*-cations in the two ligands. The three modified gold nanoclusters were designated as Au-1, Au-2, and Au-3. The absolute quantum efficiency of the gold nanoclusters increased from <0.3% after the layer-by-layer coating of the three surface ligands to 59.6% after the primary coverage and 90.3% after the secondary coverage. The fluorescence lifetime of the gold nanoclusters was also extended from 3.5 ns to 43.8 ns and 61.0 ns (Fig. 8c–e). This distribution of increasing the surface rigidity of the clusters resulted in a 3.6-fold increase in the radiative excursion rate of the clusters and a 57.4-fold decrease in the nonradiative excursion rate, which indicates that the nonradiative excursion rate during luminescence is effectively suppressed.[170]

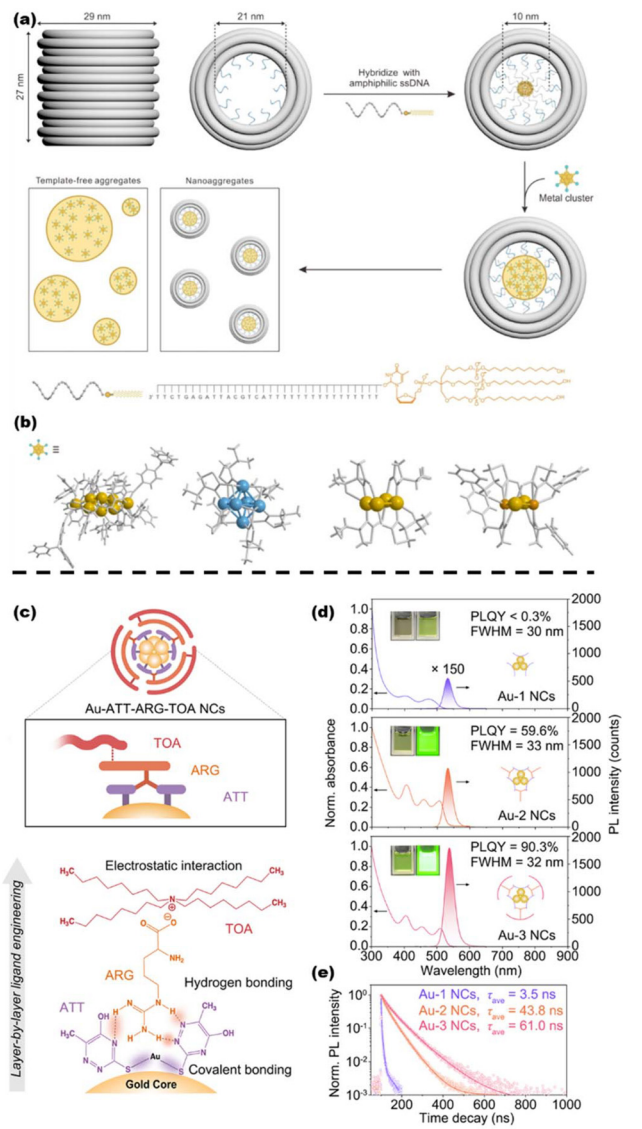

Fig. 8 (a) Design and operation of a hydrophobic alkyl core barrel DNA framework, as well as a schematic representation of the polymerization of MNCs directed by a DNA framework. (b) MNCs employed in the study and their atomic structures. Au_8, Ag_6, Au_4, and Au_2Cu_2 are arranged from left to right. Reproduced from ref. 168 with permission from the American Chemical Society, copyright (2024). (c) Schematic illustration of the layer-by-layer self-assembly evolution of triple-ligands. ATT = purple, ARG = orange, and TOA = pink. (d) UV-vis and photoluminescence spectra of Au-1, Au-2, and Au-3 nanoclusters, the insets show the digital optical photographs of Au-1, Au-2, and Au-3 under ambient conditions (left) and 365 nm excitation (right). (e) Luminescence time-resolved spectra of Au-1, Au-2, and Au-3 under 405 nm excitation. Reproduced from ref. 170 with permission from Springer Nature, copyright (2023).

4. Application in bioimaging

Based on the remarkable success of metal MNCs in near-infrared two-region (NIR-II) PL activities, it was hoped that the clusters could also feature several biocatalytic activities. However, the near-infrared emission is often accompanied by many non-radiative transitions, and the luminescence efficiency is relatively low. The biocatalytic process, on the other hand, demands electron transfer between the substrate and the catalyst, which significantly reduces the number of free electrons involved in the luminescence. Therefore, these contradictions lead to the concurrent unavailability of ideal clusters with strong luminescence and catalytic activity. Ma *et al.* have synthesized an $Au_{22}(SG)_{18}$ nanocluster with strong emission at NIR-II with glutathione. By inserting Cu monoatomic sites on the cluster surface, the resulting $Au_{21}Cu$ is 18 times more resistant to oxidation, 90 times more active as a peroxidase, and has 3 times higher superoxide dismutase activity than Au_{21} without any accompanying loss of luminescence. Thus, this cluster modulation successfully suppressed the inflammation produced in the kidneys and brain of mice under cisplatin anticancer treatment, which could be visualized by NIR-II optical microscopy[171] (Fig. 9). Meanwhile, clusters in some biological tissues where NIR emission generates the self-burst phenomenon can also be designed as special switch-type imaging probes using their interactions with intracellular sub-

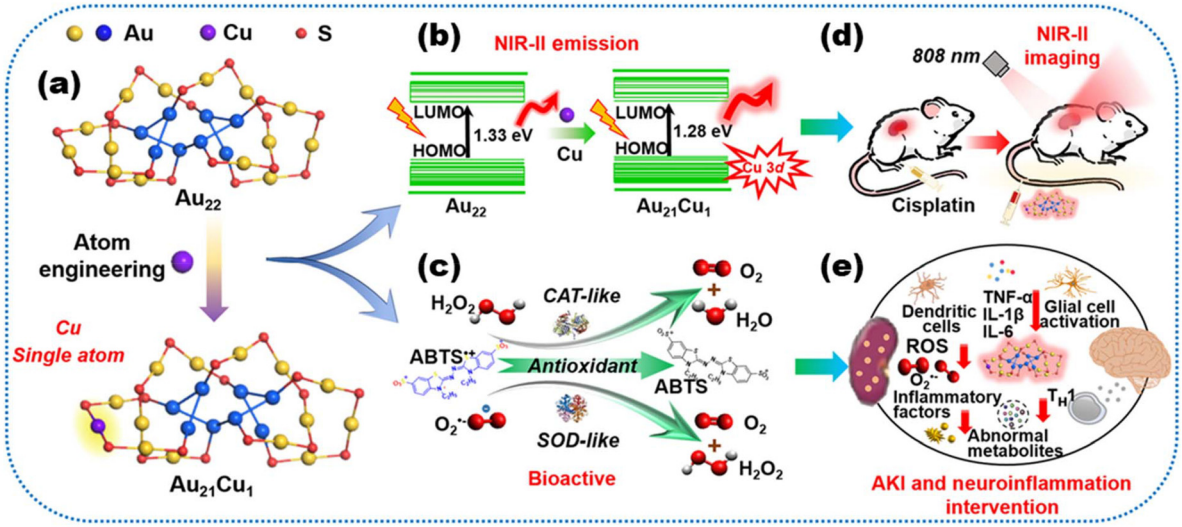

Fig. 9 Schematic diagram of the photoluminescence properties and biomedical applications of Au_{22} and $Au_{21}Cu$ nanoclusters. (a) A Cu atom active site was introduced into the Au_{22} clusters having strong NIR-II fluorescence. (b) Single-atom doping procedure reducing the energy gap from 1.33 to 1.28 eV with the contributions of the *s* and *p* states of Cu. (c) Cu atom with lost electron states contributing to potent enzyme-mimicking activities. Clusters exhibiting (d) the bioactive NIR-II behavior and (e) good capacities for highly accurate monitoring of cisplatin-induced kidney injury and inhibition of oxidative stress and inflammation in multiple organs of the cisplatin-treated mouse model, particularly in the kidneys and brain. Note: ABTS = 2,2′-azino-bis (3-ethylbenzothiazoline-6-sulfonic acid), CAT = hydrogen peroxidase, SOD = superoxide dismutase, TNF-α = tumor necrosis factor α, IL = interleukin, ROS = reactive oxygen species, and AKI = acute kidney injury. Reproduced from ref. 171 with permission from the American Association for the Advancement of Science, copyright (2023).

stances. Activatable fluorescent nanoprobes with only one nanomaterial that can act as both energy donors and acceptors are scarce, but highly needed for biosensing and bioimaging. Yan *et al.* enabled highly sensitive and selective intracellular imaging of glutathione amounts in gold nanoclusters that were originally self-bursting through the interaction between ligands on the surface of the clusters and intracellular glutathione.[172]

In addition to sensing glutathione composition *in vivo*, optical probes also play an essential role in sensing other significant indicators of intracellular environmental factors, such as pH and temperature. Sedghi *et al.* synthesized, for the first time, insulin-protected AuAg bimetallic nanoclusters with dual emission properties (410 nm/630 nm). It was revealed that the two emission peaks were attributed to the formation of cross-linked di-tyrosine and bimetallic nanoclusters, respectively, and that each emission peak was able to respond to one of the variables in the cell while keeping the other emission peak constant. With this property, they have obtained a linear range of intracellular pH in the range of 6.0–9.0 and temperature in the range of 1–71 °C, which can be successfully applied to direct ratiometric pH and temperature probes. This bimetallic optical nanoprobe can differentiate between tumor cells and normal cells.[173] The development of reliable probes to accurately monitor metabolic processes arising in living systems with high sensitivity and selectivity is essential to elucidate their function in many life-threatening diseases and to improve therapeutic interventions. Liu *et al.* developed a new cluster-based nanoprobe using electrostatic interactions between two gold nanoclusters. The FRET interaction between the two clusters conferred excellent single excitation/dual emission fluorescence properties (470 nm/685 nm) and showed a quantitative ratiometric fluorescence response to $ONOO^-$. The $ONOO^-$ concentration range with favorable linearity between the emission intensity ratios at 685 and 470 nm was 0–100 μM, with a detection limit (LOD) of 0.39 μM. The possible mechanism of the fluorescence response is attributed to the combined effect of the dissociation-disturbed FRET and reconstruction of the surface structure. It was efficiently used for bioimaging and monitoring exogenous and endogenous $ONOO^-$ levels in live cells and zebrafish with high contrast.[174] Another example is zearalenone (ZEN), which is a fungal secondary metabolite, and its presence is potentially hazardous to human and animal health. Wang *et al.* selected DNA-templated silver nanoclusters and the metal–organic framework (MOF) material MIL-101 to act as energy donor–acceptor pairs in the FRET process. The π···π stacking between the clusters and the MOF material resulted in PL bursting of the clusters. However, ZEN can disrupt the situation, which brings about the recovery of luminescence. This behavior can be used to indicate the concentration of ZEN in the organism.[175]

Owing to their excellent biocompatibility, MNCs have recently begun to be increasingly employed in *in vivo* tissue and organ imaging. Owing to the ease of bursting in the digestive microenvironment, Li *et al.* realized a high quantum yield with NIR-II (1050 nm) by designing the encapsulation of gold nanoclusters using a protein corona structure consisting of ribonuclease-A (RNase-A). This optical probe material is more

than 50 times as sensitive in the gastrointestinal tract as other luminescent materials such as rare earth elements. When the probe moves with gastrointestinal peristalsis, it allows the detailed structure of the gastrointestinal tract to be observed.[176] Furthermore, based on effective luminescence detection, the use of clusters for cellular drug delivery is also being attempted. Le Guével *et al.* utilized cationic polymers to mediate the loading of several peptides and antibodies during the self-assembly of gold nanoclusters, which were demonstrated to improve the delivery of drugs.[177] Meanwhile, MNCs have been investigated further in the diagnosis and treatment of some diseases. Immunotherapy is an advanced cancer treatment strategy, but there exists a lack of relevant technologies for real-time monitoring. Yuan *et al.* externalized the immune checkpoint inhibitor 1-cyclohexyl-2-(5*H*-imidazo[5,1-a]isoindol-5-yl)ethanol (NLG919) on the surface of the classical NIR-II-photoluminescent gold nanocluster $Au_{44}MBA_{26}$ (MBA = water-soluble 4-mercaptobenzoic acid) to form $Au_{44}MBA_{26}$–NLG. The clusters were irradiated with near-infrared light to produce singlet oxygen ($^1O_2$), leading to cleavage at the junction and

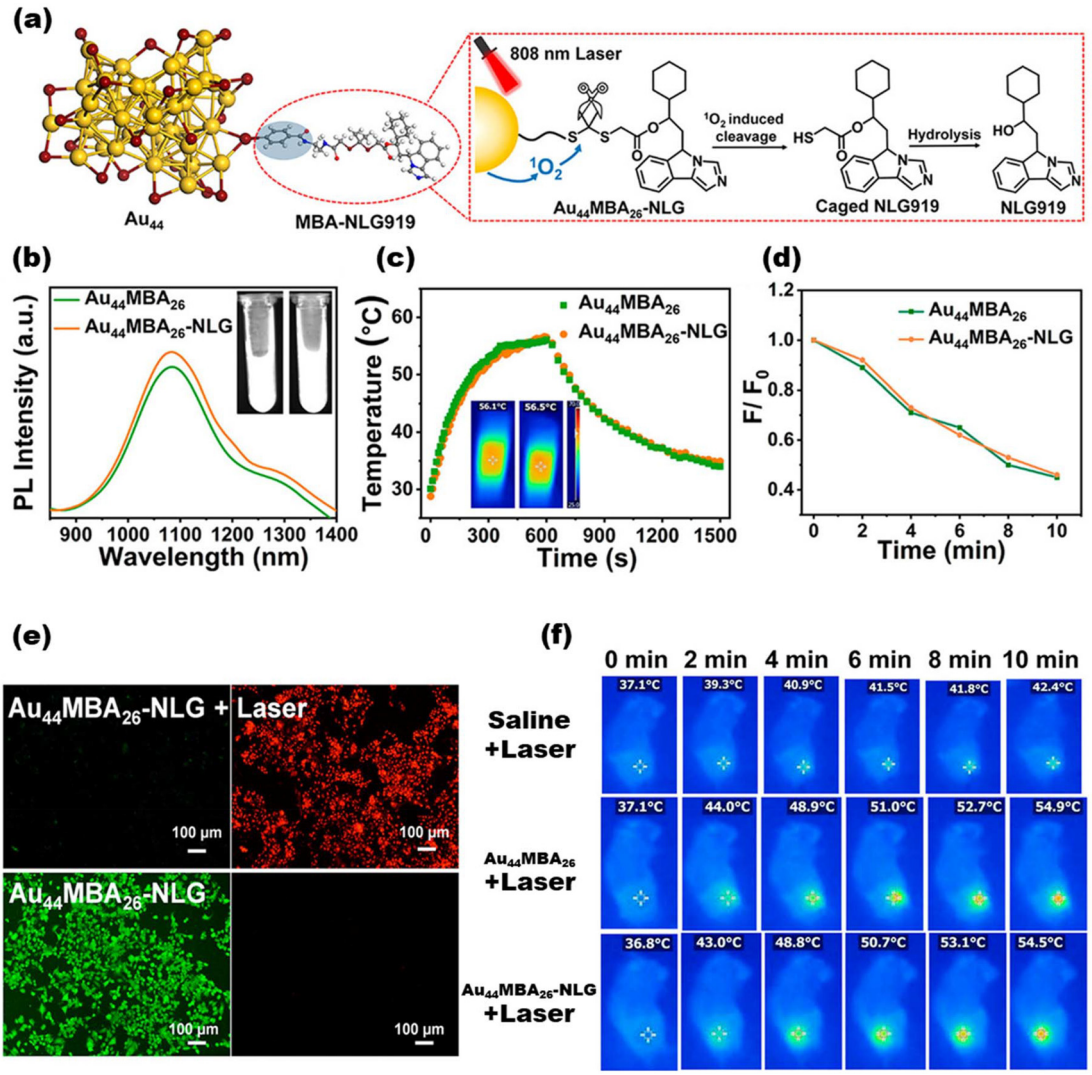

Fig. 10 (a) Crystal structure of the $Au_{44}MBA_{26}$ nanocluster and the targeting principle of NIR photoactivated $Au_{44}MBA_{26}$–NLG. (b) Photoluminescence spectra of $Au_{44}MBA_{26}$ and $Au_{44}MBA_{26}$–NLG (λ_{exc} = 808 nm). Note: the inset displays the photos of $Au_{44}MBA_{26}$ (left) and $Au_{44}MBA_{26}$–NLG solutions (right) under NIR excitation. (f) Photothermal temperature curves of $Au_{44}MBA_{26}$ and $Au_{44}MBA_{26}$–NLG as a function of laser irradiation time (λ_{exc} = 808 nm, 1.5 W cm^{-2}, *c* (MNCs) = 60 μM). Note: the inset displays the IR thermal images of $Au_{44}MBA_{26}$ (left) and $Au_{44}MBA_{26}$–NLG (right) at the corresponding highest temperatures. (d) The relative productivity of $^1O_2$ over $Au_{44}MBA_{26}$ and $Au_{44}MBA_{26}$–NLG as a function of laser irradiation time. (e) Confocal laser scanning microscopic images of $Au_{44}MBA_{26}$–NLG treated 4T1 cells under excitation at 808 nm (top panel) for 6 min (1.5 W cm^{-2}) and under dark conditions (lower panel). Note: non-viable 4T1 cells are stained red with ethidium homodimer-1 (EthD-1) and viable cells are stained green with calcein AM. (f) Thermal pictures of 4T1 tumor-bearing mice exposed to 808 nm laser irradiation for 10 minutes (1.0 W cm^{-2}) after intravenous injections of saline, $Au_{44}MBA_{26}$, and $Au_{44}MBA_{26}$–NLG. Reproduced from ref. 178 with permission from the American Chemical Society, copyright (2023).

release of the drug molecules. $Au_{44}MBA_{26}$–NLG is capable of NIR-II PL imaging of tumors in deep tissues to guide tumor therapy as well as performing corresponding photodynamic therapy. The multiple effects of $Au_{44}MBA_{26}$–NLG promote the proliferation and activation of effector T cells and ultimately inhibit the growth of primary and distant tumors in living mice[178] (Fig. 10).

It has recently been recognized that optical imaging of metal nanoclusters in NIR-II holds great promise for deep tissue visualization. In particular, gold nanoclusters, the most novel clinically translatable NIR-II probes, have demonstrated strong capabilities in bone imaging. Cheng *et al.* first discovered the efficient binding ability of $Au_{25}(SG)_{18}$ nanoclusters to hydroxyapatite. The *in vivo* NIR-II optical imaging results demonstrated that the clusters aggregated in bone tissue with high contrast and signal-to-background ratios, showing excellent imaging of ribs and thoracic vertebrae, as well as rapid excretion through the renal system.[179] A further step, the exploitation of composite optical probes for non-invasive bone imaging and related disease diagnosis, has been pursued. Yuan *et al.* have once again utilized atomically precise NIR-II-emitting Au_{44} nanoclusters as templates for specific targeting moiety loading *via* surface phosphorylation reactions. Thanks to the highly concentrated phosphate groups, this phosphorylation strengthens the bone-targeting ability of the optical probe, enabling the probe to perform *in vivo* bone-targeted NIR-II PL imaging. Besides, with enhanced bone targeting ability, an ultra-small hydrodynamic diameter, and excellent anti-inflammatory and immunomodulatory effects, the probe not only exhibits superior therapeutic efficacy for rheumatoid arthritis (RA) in rats, effectively restoring damaged cartilage to near-normal, but also demonstrates excellent renal clearance and benign biocompatibility. In contrast, commercial methotrexate, commonly used in RA therapy, is unable to achieve these favorable properties[180] (Fig. 11). Also, the toxicity and photostability of the probes were thoroughly evaluated to ensure that they satisfy imaging demands before the bioimaging experiments. Moreover, the probe molecules usually have to be maintained for a long duration of time under simulated *in vivo* conditions.

Very recently, due to advances in understanding the photophysics and molecular dynamics of fluorophores at the single-molecule level, single-molecule fluorescence imaging and spectroscopy have attracted much attention. It is difficult to develop fluorescent compounds utilizing single-molecule approaches for real-time spectroscopic observation in biological environments. Single-molecule spectroscopy (SMS) is a unique and effective technique for studying molecular dynamics and accurately sensing biomolecules. Patra *et al.* have found that $AuAg_{28}$ has better photostability than the Ag_{29} nanocluster. Doping enables MNCs to exhibit superior brightness and excellent photostability in photon antipolymerization beam experiments, surviving for up to 218 seconds and exhibiting a longer "on" time and shorter "off" time.[181] Furthermore, Nandi *et al.* synthesized a red-emitting gold nanocluster capable of coupling with proteins. They utilized super-resolution microscopy (SRM) to observe super-resolution radial fluctuations (SRRFs) of lysosomes in HeLa cells that were very close to the original diameter of the smallest lysosomes in HeLa cells.[182]

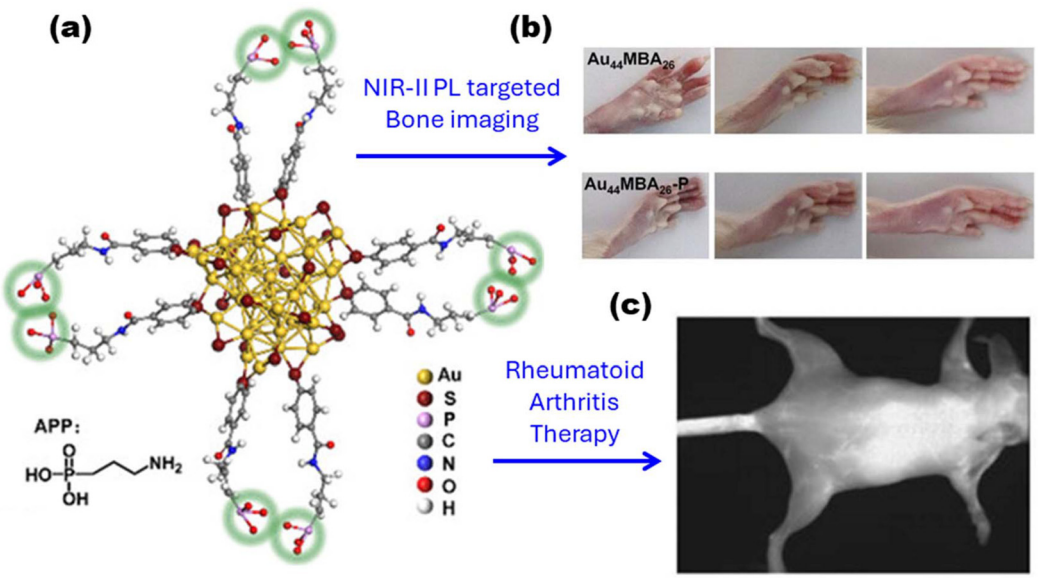

Fig. 11 (a) Crystal structure and schematic illustration of the $Au_{44}MBA_{26}$–P probe. Note: the phosphate groups are labeled with green circles, and only partial ligands are shown for clarity. (b) Pictures showing representative samples of healthy rats at the beginning, middle, and end of the drug administration period, as well as collagen-induced arthritis (CIA) rats treated with $Au_{44}MBA_{26}$, and $Au_{44}MBA_{26}$–P nanoclusters. (c) Targeting specific bone with the $Au_{44}MBA_{26}$–P nanocluster at high resolution *in vivo*. Reproduced from ref. 180 with permission from Wiley, copyright (2024).

5. Perspectives and conclusion

Until now, MNCs have received much attention as a new class of optical probe materials in bioimaging. At this stage, various types of metal nanoclusters have been successfully applied to cellular and biological tissue imaging based on their excellent near-infrared emission, and some of them have been initially explored for clinical diagnosis and treatment. However, there are still some challenges to be solved in the research.

5.1. Luminescence quenching in biological aqueous phase environments

Most organic optical probes suffer from aggregation-induced quenching (ACQ) effects.[183] Therefore, from the very beginning of the deployment of clusters in optical bioimaging (until now), the cluster-based optical probes selected and synthesized were still focused on water-soluble metal nanoclusters. In most cases, the ligands chosen were organic ligands such as DNA and peptides,[184,185] which are very biocompatible and water-soluble. This approach completely solves the problem of ACQ but poses other problems. Water-soluble MNCs are often not readily identified with precise structures owing to their difficulties in crystallization, even when the single component is identified by mass spectrometry. Of course, many water-soluble MNCs have demonstrated excellent imaging capabilities, but it is difficult to give a precise interpretation of the optical behavior of the probe from the molecular-level perspective. This makes it extremely difficult to design specific working modes for probes later on.

5.2. Targeting

At present, the requirements for optical probes are gradually tending to be target-oriented and functionalized. This requires the corresponding optical probes to be capable of not only successful luminescence *in vivo*, but also accurate luminescence in a specific location. The feedback of such demands on cluster synthesis is that specific targeting groups should be embedded in the exterior of the clusters without affecting the normal luminescence activity of the clusters. While some researchers have now begun to make such attempts,[186,187] there is not yet a systematic synthetic method for targeting functionalization to specific organelles, tissues, organs, *etc*.

5.3. Multi-mode optical imaging

In the reported cases, the existing probe modes of clusters still focus on the "always-on" mode, that is, the probe is in the bright state during operation all the time. In contrast, the "off" mode implies an inductive bursting of the probe during the imaging process. However, for real-time observation of various sensing processes in organisms, optical probes with more sophisticated imaging modes such as "off–on", "on–off", and "on–off–on", *etc*. might be desirable.[188,189]

In summary, the remarkably rich optical behaviors and flexible modulations regarding MNCs are highlighted in this mini-review. Based on these detailed foundations, this mini-review summarizes some favorable performances of metal nanoclusters as optical probes in bioimaging and related disease diagnosis and treatment. This research field is still in its infancy and suffers from some of the problems mentioned above, but there are already some practicable solutions. With a deeper understanding of the optical properties of metal nanoclusters and the maturity of related synthesis and modification methods, they will play a more powerful role as novel optical probes.

Data availability

No primary research results, software, or code have been included and no new data were generated or analysed as part of this review.

Conflicts of interest

There are no conflicts to declare.

Acknowledgements

This work was financially supported by the National Natural Science Foundation of China (22303001, 22371002, and 92061110), the Anhui University Startup Fund (S020318006/022), and the Anhui Provincial Natural Science Foundation (2108085Y05).

References

1 S. Yoon, M. Kim, M. Jang, Y. Choi, W. Choi, S. Kang and W. Choi, *Nat. Rev. Phys.*, 2020, **2**, 141–158.
2 A. J. Wilson, D. Devasia and P. K. Jain, *Chem. Soc. Rev.*, 2020, **49**, 6087–6112.
3 Y. Jiang and K. Pu, *Chem. Rev.*, 2021, **121**, 13086–13131.
4 L. Mennel, M. M. Furchi, S. Wachter, M. Paur, D. K. Polyushkin and T. Mueller, *Nat. Commun.*, 2018, **9**, 516.
5 F. Hu, C. Zeng, R. Long, Y. Miao, L. Wei, Q. Xu and W. Min, *Nat. Methods*, 2018, **15**, 194–200.
6 Y.-C. Chen, A. E. Jablonski, I. Issaeva, D. Bourassa, J.-C. Hsiang, C. J. Fahrni and R. M. Dickson, *J. Am. Chem. Soc.*, 2015, **137**, 12764–12767.
7 J. Zhao, Z. Li, Y. Shao, W. Hu and L. Li, *Angew. Chem., Int. Ed.*, 2021, **60**, 17937–17941.
8 J. Qian, Z. Feng, X. Fan, A. Kuzmin, A. S. L. Gomes and P. N. Prasad, *Phys. Rep.*, 2022, **962**, 1–107.
9 S. Osella and S. Knippenberg, *J. Am. Chem. Soc.*, 2017, **139**, 4418–4428.
10 K. Y. Duan and B. Liu, *Adv. Mater.*, 2018, **30**, 1870361.
11 I. Martinić, S. V. Eliseeva, T. N. Nguyen, V. L. Pecorao and S. Petoud, *J. Am. Chem. Soc.*, 2017, **139**, 8388–8391.
12 J. Huang, J. Li, Y. Lyu, Q. Miao and K. Pu, *Nat. Mater.*, 2019, **18**, 1133–1143.

13 M. Bertolini, M. S. Wong, L. M. Tapia and M. Vendrell, *Chem. Soc. Rev.*, 2023, **52**, 5352–5372.
14 Y.-L. Qi, Y.-Z. Li, M.-J. Tan, F.-F. Yuan, N. Murthy, Y.-T. Duan, H.-L. Zhu and S.-Y. Yang, *Coord. Chem. Rev.*, 2023, **486**, 215130.
15 Y. Su, B. Yu, S. Wang, H. Cong and Y. Shen, *Biomaterials*, 2021, **271**, 120717.
16 R. Zhai, B. Fang, Y. Lai, B. Peng, H. Bai, X. Liu, L. Li and W. Huang, *Chem. Soc. Rev.*, 2023, **52**, 942–972.
17 A. Mahajan and T. S. Chundawat, *Mini-Rev. Org. Chem.*, 2019, **16**, 631–652.
18 H. Li, Y. Kim, H. Jung, J. Y. Hyun and I. Shin, *Chem. Soc. Rev.*, 2022, **51**, 8957–9008.
19 Q. Shen, L. Wang, X. Ruan, N. Li, W. Wang, W. Wang, J. Shao and X. Dong, *Adv. Funct. Mater.*, 2023, **33**, 2300023.
20 H. Chen, L. Liu, K. Qian, H. Liu, Z. Wang, F. Gao, C. Qu, W. Dai, D. Lin, K. Chen, H. Liu and Z. Cheng, *Sci. Adv.*, 2022, **8**, eabo3289.
21 Z. Yang, C. Zhang, W. Zhang, J. Zhong, H. Wu, K. Wang and J. Cao, *Chem. Eng. J.*, 2024, **496**, 153741.
22 J. V. Jun, D. M. Chenoweth and E. J. Petersson, *Org. Biomol. Chem.*, 2020, **18**, 5747–5763.
23 H.-H. Han, H. Tian, Y. Zang, A. C. Sedgwick, J. Li, J. L. Sessler, X.-P. He and T. D. James, *Chem. Soc. Rev.*, 2021, **50**, 9391–9429.
24 M. Minoshima, S. I. Reja, R. Hashimoto, K. Lijima and K. Kikuchi, *Chem. Rev.*, 2024, **124**, 6198–6270.
25 C. Ding and T. Ren, *Coord. Chem. Rev.*, 2023, **482**, 215080.
26 S.-Y. Chen, Z. Li, K. Li and X.-Q. Yu, *Coord. Chem. Rev.*, 2021, **429**, 213691.
27 H. Singh, K. Tiwari, R. Tiwari, S. K. Pramanik and A. Das, *Chem. Rev.*, 2019, **119**, 11718–11760.
28 P. K. S. Magut, S. Das, V. E. Fernand, J. Losso, K. McDonoughm, B. M. Naylor, S. Aggarwal and I. M. Warner, *J. Am. Chem. Soc.*, 2013, **135**, 15873–15879.
29 W. Liu, J. Chen and Z. Xu, *Coord. Chem. Rev.*, 2021, **429**, 213638.
30 K. K.-W. Lo, *Acc. Chem. Res.*, 2020, **53**, 32–44.
31 S. Li, J. Wei, Q. Yao, X. Song, J. Xie and H. Yang, *Chem. Soc. Rev.*, 2023, **52**, 1672–1696.
32 A. Chaix, E. Cueto-Diaz, S. Dominguez-Gil, C. Spiteri, L. Lichon, M. Maynadier, X. Dumail, D. Aggad, A. Delalande, A. Bessière, C. Pichon, C. Chiappini, M. J. Sailor, N. Bettache, M. Gary-Bobo, J.-O. Durand and C. Nguyen, *Adv. Healthcare Mater.*, 2023, **12**, 2301052.
33 C. J. Murphy, A. M. Gole, J. W. Stone, P. N. Sisco, A. M. Alkilany, E. C. Goldsmith and S. C. Baxter, *Acc. Chem. Res.*, 2008, **41**, 1721–1730.
34 M. C. Dos Santos, I. Colin, G. R. Dos Santos, K. Susumu, M. Demarque, I. L. Medintz and N. Hildebrandt, *Adv. Mater.*, 2020, **32**, 2003912.
35 D. Liu, H. He, F. Kong, Y. Cao, F. Zang, M. Ma, N. Gu and Y. Zhang, *Nano Today*, 2022, **47**, 101689.
36 Y. Wang, W. Zhang, P. Sun, Y. Cai, W. Xu, Q. Fan, Q. Hu and W. Han, *Theranostics*, 2019, **9**, 391–404.
37 Y.-C. Ou, X. Wen and R. Bardhan, *Trends Biotechnol.*, 2020, **38**, 388–403.
38 R. Savla and T. Minko, *Adv. Drug Delivery Rev.*, 2017, **113**, 122–140.
39 S. H. Lim, T. W. Wong and W. X. Tay, *Adv. Colloid Interface Sci.*, 2024, **325**, 103094.
40 Z. Zhao, K. He, B. Liu, W. Nie, X. Luo and J. Liu, *Angew. Chem., Int. Ed.*, 2024, **63**, e202406016.
41 F. Oroojalian, F. Charbgoo, M. Hashemi, A. Amani, R. Yazdian-Robati, A. Mokhtarzadeh, M. Ramezani and M. R. Hamblin, *J. Controlled Release*, 2020, **321**, 442–462.
42 Q. Yao, T. Chen, X. Yuan and J. Xie, *Acc. Chem. Res.*, 2018, **51**, 1338–1348.
43 Y. Li, M. Zhou and R. Jin, *Adv. Mater.*, 2021, **33**, 2006591.
44 M. F. Matus and H. Häkkinen, *Nat. Rev. Mater.*, 2023, **8**, 372–389.
45 M. F. Matus and H. Häkkinen, *Small*, 2021, **17**, 2170140.
46 Y. Zheng, J. Wu, H. Jiang and X. Wang, *Coord. Chem. Rev.*, 2021, **431**, 213689.
47 S. M. Farkhani, P. Dehghankelishadi, A. Refaat, D. V. Gopal, A. Cifuentes-Rius and N. H. Voelcker, *Prog. Mater. Sci.*, 2024, **142**, 101229.
48 S. Zhou, B. Peng, Y. Duan, K. Liu, O. Ikkala and R. H. A. Ras, *Angew. Chem., Int. Ed.*, 2022, **61**, e202210808.
49 T. Chen, H. Lin, Y. Cao, Q. Yao and J. Xie, *Adv. Mater.*, 2022, **34**, 2103918.
50 Y. Cai, Z. Wei, C. Song, C. Tang, W. Han and X. Dong, *Chem. Soc. Rev.*, 2019, **48**, 22.
51 J. Kong, W. Zhang, Y. Wu and M. Zhou, *Aggregate*, 2022, **3**, e207.
52 M. Zhou, T. Higaki, Y. Li, C. Zeng, Q. Li, M. Y. Sfeir and R. Jin, *J. Am. Chem. Soc.*, 2019, **141**, 19754–19764.
53 Z. Lin, N. Goswami, T. Xue, O. J. H. Chai, H. Xu, Y. Liu, Y. Su and J. Xie, *Adv. Funct. Mater.*, 2021, **31**, 2105662.
54 M. Guo, G. Zhang, R. Zhao, H. Ma, Y. Yan, S. Yang, J. Meng, Y. Huang, X.-D. Zhang, H. Wang and R. Zhang, *ACS Appl. Nano Mater.*, 2023, **6**, 15945–15958.
55 X. Jiang, B. Du, S. Tang, J.-T. Hsieh and J. Zheng, *Angew. Chem., Int. Ed.*, 2019, **58**, 5994–6000.
56 Y. Shi, Z. Wu, M. Qi, C. Liu, W. Dong, W. Sun, X. Wang, F. Jiang, Y. Zhong, D. Nan, Y. Zhang, C. Li, L. Wang and X. Bai, *Adv. Mater.*, 2024, **36**, 2310529.
57 Z. Lin, N. Goswami, T. Xue, O. J. H. Chai, H. Xu, Y. Liu, Y. Su and J. Xie, *Adv. Funct. Mater.*, 2021, **31**, 2105662.
58 X. Kang, Y. Li, M. Zhu and R. Jin, *Chem. Soc. Rev.*, 2020, **49**, 6443–6514.
59 E. L. Albright, T. I. Levchenko, V. K. Kulkarni, A. I. Sullivan, J. F. DeJesus, S. Malola, S. Takano, M. Nambo, K. Stamplecoskie, H. Häkkinen, T. Tsukuda and C. M. Crudden, *J. Am. Chem. Soc.*, 2024, **146**, 5759–5780.
60 X. Tang, H. Shen, H. Huang, L. Li, F. Luo, G. Tian, H. Deng, B. K. Teo and N. Zheng, *Small Methods*, 2024, 202400040.
61 Y. Zhang, W. Zhang, T.-S. Zhang, C. Ge, Y. Tao, W. Fei, W. Fan, M. Zhou and M.-B. Li, *J. Am. Chem. Soc.*, 2024, **146**, 9631–9639.

62 X. Zou, X. Kang and M. Zhu, *Chem. Soc. Rev.*, 2023, **52**, 5892–5967.
63 Y. Xiao, Z. Wu, Q. Yao and J. Xie, *Aggregate*, 2021, **2**, 114–132.
64 G. Yang, Z. Wang, F. Du, F. Jiang, X. Yuan and J. Y. Ying, *J. Am. Chem. Soc.*, 2023, **145**, 11879–11898.
65 M. J. Mitchell, M. M. Billingsley, R. M. Haley, M. E. Wechsler, N. A. Peppas and R. Langer, *Nat. Rev. Drug Discovery*, 2021, **20**, 101–124.
66 D. Bain, Mimansa, A. Devi, S. Maity, A. Shanavas and A. Patra, *ACS Sustainable Chem. Eng.*, 2022, **10**, 12730–12737.
67 X. Yang, M. Yang, B. Pang, M. Vara and Y. Xia, *Chem. Rev.*, 2015, **115**, 10410–10488.
68 K. Pyo, N. H. Ly, S. Y. Yoon, Y. Shen, S. Y. Choi, S. Y. Lee, S.-W. Joo and D. Lee, *Adv. Healthcare Mater.*, 2017, **6**, 1700203.
69 F. Xu, T. Qing and Z. Qing, *Nano Today*, 2021, **36**, 101021.
70 R. T. K. Kwok, B. Liu and B. Z. Tang, *Adv. Opt. Mater.*, 2020, **8**, 2000855.
71 Y. Zhang, S.-R. He, Y. Yang, T.-S. Zhang, Z.-M. Zhu, W. Fei and M.-B. Li, *J. Am. Chem. Soc.*, 2023, **145**, 12164–12172.
72 R. Jin, *Nanoscale*, 2015, **7**, 1549–1565.
73 M. Zhu, C. M. Aikens, F. J. Hollander, G. C. Schatz and R. Jin, *J. Am. Chem. Soc.*, 2008, **130**, 5883–5885.
74 J. Zheng, P. R. Nicovich and R. M. Dickson, *Annu. Rev. Phys. Chem.*, 2007, **58**, 409–431.
75 W. Ishii, Y. Okayasu, Y. Kobayashi, R. Tanaka, S. Katao, Y. Nishikawa, T. Kawai and T. Nakashima, *J. Am. Chem. Soc.*, 2023, **145**, 11236–11244.
76 Z. Wu and R. Jin, *Nano Lett.*, 2010, **10**, 2568–2573.
77 Y. Song, J. Zhong, S. Yang, S. Wang, T. Cao, J. Zhang, P. Li, D. Hu, Y. Pei and M. Zhu, *Nanoscale*, 2014, **6**, 13977–13985.
78 L. Zhang and E. Wang, *Nano Today*, 2014, **9**, 132–157.
79 H.-R. Fu, L.-B. Yan, N.-T. Wu, L.-F. Ma and S.-Q. Zang, *J. Mater. Chem. A*, 2018, **6**, 9183–9191.
80 G. Sun, H. Cui, L. Y. Lin, N. S. Lee, C. Yang, W. L. Neumann, J. N. Freskos, J. J. Shieh, R. B. Dorshow and K. L. Wooley, *J. Am. Chem. Soc.*, 2011, **133**, 8534–8543.
81 M. Kawashiro, T. Mori, M. Ito, N. Ando and S. Yamaguchi, *Angew. Chem., Int. Ed.*, 2023, **62**, e202303725.
82 F. W. Pratiwi, C.-H. Hsia, C. W. Kuo, S.-M. Yang, Y.-K. Hwu and P. Chen, *Biosens. Bioelectron.*, 2016, **84**, 133–140.
83 Z.-M. Ying, Z. Wu, B. Tu, W. Tan and J.-H. Jiang, *J. Am. Chem. Soc.*, 2017, **139**, 9779–9782.
84 L. Wu, I.-C. Wu, C. C. DuFort, M. A. Carlson, X. Wu, L. Chen, C.-T. Kuo, Y. Qin, J. Yu, S. R. Hingorani and D. T. Chiu, *J. Am. Chem. Soc.*, 2017, **139**, 6911–6918.
85 R. Gui, H. Jin, X. Bu, Y. Fu, Z. Wang and Q. Liu, *Coord. Chem. Rev.*, 2019, **383**, 82–103.
86 M. B. Liisberg, V. Rück, G. Romolini, C. Cerretani and T. Vosch, *Adv. Opt. Mater.*, 2024, **12**, 2400345.
87 W. Wei, Y. Lu, W. Chen and S. Chen, *J. Am. Chem. Soc.*, 2011, **133**, 2060–2063.
88 Q. Li, D. Zhou, J. Chai, W. Y. So, T. Cai, M. Li, L. A. Peteanu, O. Chen, M. Cotlet, X. W. Gu, H. Zhu and R. Jin, *Nat. Commun.*, 2020, **11**, 2897.
89 S. Wang, X. Meng, A. Das, T. Li, Y. Song, T. Cao, X. Zhu, M. Zhu and R. Jin, *Angew. Chem., Int. Ed.*, 2014, **53**, 2376–2380.
90 L. Luo, Z. Liu, X. Du and R. Jin, *J. Am. Chem. Soc.*, 2022, **144**, 19243–19247.
91 M. B. Liisberg, S. Krause, C. Cerretani and T. Vosch, *Chem. Sci.*, 2022, **13**, 5582–5587.
92 C. Fang, C. Xu, W. Zhang, M. Zhou, D. Tan, L. Qian, D. Hu, S. Jin and M. Zhu, *Nat. Commun.*, 2024, **15**, 5962.
93 X.-J. Zhang, M.-E. Sun, F. Sun, Y. Jin, X.-Y. Dong, S. Li, H.-Y. Li, G. Chen, Y. Fu, Y. Wang, Q. Tang, Y. Wu, L. Jiang and S.-Q. Zang, *Angew. Chem., Int. Ed.*, 2024, **63**, e202401724.
94 M. B. Liisberg, V. Rück, G. Romolini, C. Cerretani and T. Vosch, *Adv. Opt. Mater.*, 2024, **12**, 2400345.
95 S. Malolaa and H. Häkkinen, *Chem. Commun.*, 2024, **60**, 3315–3318.
96 Y. Chen, J. W. Y. Lam, R. T. K. Kwok, B. Liu and B. Z. Tang, *Mater. Horiz.*, 2019, **6**, 428–433.
97 Y. Tu, Z. Zhao, J. W. Y. Lam and B. Z. Tang, *Natl. Sci. Rev.*, 2021, **8**, nwaa260.
98 F.-Y. Zhu, L.-J. Mei, R. Tian, C. Li, Y.-L. Wang, S.-L. Xiang, M.-Q. Zhu and B. Z. Tang, *Chem. Soc. Rev.*, 2024, **53**, 3350–3383.
99 Y.-J. Kong, Z.-P. Yan, S. Li, H.-F. Su, K. Li, Y.-X. Zheng and S.-Q. Zang, *Angew. Chem., Int. Ed.*, 2020, **59**, 5336–5340.
100 Z. Luo, X. Yuan, Y. Yu, Q. Zhang, D. T. Leong, J. Y. Lee and J. Xie, *J. Am. Chem. Soc.*, 2012, **134**, 16662–16670.
101 N. Goswami, Q. Yao, Z. Luo, J. Li, T. Chen and J. Xie, *J. Phys. Chem. Lett.*, 2016, **7**, 962–975.
102 D. Bain, S. Maity and A. Patra, *Chem. Commun.*, 2020, **56**, 9292–9295.
103 Z. Wu, J. Liu, Y. Gao, H. Liu, T. Li, H. Zou, Z. Wang, K. Zhang, Y. Wang, H. Zhang and B. Yang, *J. Am. Chem. Soc.*, 2015, **137**, 12906–12913.
104 S. Chakraborty, D. Bain, S. Maity, S. Kolay and A. Patra, *J. Phys. Chem. C*, 2022, **126**, 2896–2904.
105 D. Bain, S. Maitya and A. Patra, *Phys. Chem. Chem. Phys.*, 2019, **21**, 5863–5881.
106 S. Maity, D. Bain and A. Patra, *J. Phys. Chem. C*, 2019, **123**, 2506–2515.
107 S. Maity, D. Bain and A. Patra, *Nanoscale*, 2019, **11**, 22685–22723.
108 Z. Wu, Q. Yao, S.-Q. Zang and J. Xie, *Natl. Sci. Rev.*, 2021, **8**, nwaa208.
109 X. Kang, S. Wang and M. Zhu, *Chem. Sci.*, 2018, **9**, 3062–3068.
110 J. Xin, J. Xu, C. Zhu, Y. Tian, Q. Zhang, X. Kang and M. Zhu, *Chem. Sci.*, 2023, **14**, 8474–8482.
111 Y. Zou, M. Yu, Y. Xu, Z. Xiao, X. Song, Y. Hu, Z. Xu, C. Zhong, J. He, X. Cao, K. Li, J. Miao and C. Yang, *Chem*, 2024, **10**, 1485–1501.
112 M. A. Brydena and E. Zysman-Colman, *Chem. Soc. Rev.*, 2021, **50**, 7587–7680.

113 D. S. M. Ravinson and M. E. Thompson, *Mater. Horiz.*, 2020, **7**, 1210–1217.
114 Z.-R. Yuan, Z. Wang, B.-L. Han, C.-K. Zhang, S.-S. Zhang, Z.-Y. Zhu, J.-H. Yu, T.-D. Li, Y.-Z. Li, C.-H. Tung and D. Sun, *Angew. Chem.*, 2022, **134**, e202211628.
115 X. Zhou, R. Ikura, C. Jin, K. Yamaoka, J. Park and Y. Takashima, *Aggregate*, 2024, **5**, e457.
116 Q. Wu, K. Y. Zhang, P. Dai, H. Zhu, Y. Wang, L. Song, L. Wang, S. Liu, Q. Zhao and W. Huang, *J. Am. Chem. Soc.*, 2020, **142**, 1057–1064.
117 P. T. Burks, A. D. Ostrowski, A. A. Mikhailovsky, E. M. Chan, P. S. Wagenknecht and P. C. Ford, *J. Am. Chem. Soc.*, 2012, **134**, 13266–13275.
118 W. R. Algar, A. Khachatrian, J. S. Melinger, A. L. Huston, M. H. Stewart, K. Susumu, J. B. Blanco-Canosa, E. Oh, P. E. Dawson and L. Medintz, *J. Am. Chem. Soc.*, 2017, **139**, 363–372.
119 Q. Dai, Z. Zhang, B. Yu, X. Li, J. Li, Z. Qi, H. He, F. Huang and X. Wang, *Nano Res.*, 2023, **16**, 12207–12214.
120 L. Wu, C. Huang, B. P. Emery, A. C. Sedgwick, S. D. Bull, X.-P. He, H. Tian, J. Yoon, J. L. Sessler and T. D. James, *Chem. Soc. Rev.*, 2020, **49**, 5110–5139.
121 T. Ha, J. Fei, S. Schmid, N. K. Lee, R. L. Gonzalez Jr, S. Paul and S. Yeou, *Nat. Rev. Methods Primers*, 2024, **4**, 21.
122 K. Pyo, M. F. Matus, E. Hulkko, P. Myllyperkiö, S. Malola, T. Kumpulainen, H. Häkkinen and M. Pettersson, *J. Am. Chem. Soc.*, 2023, **145**, 14697–14704.
123 H. Li, T. Wang, J. Han, Y. Xu, X. Kang, X. Li and M. Zhu, *Nat. Commun.*, 2024, **15**, 5351.
124 D. Li, X. Deng, Z. Xu, D. Wang, G. Xu, P. Zhang, P. Qiu, W. Xie, D. Wang, B. Z. Tang and K. Wang, *Adv. Funct. Mater.*, 2023, **33**, 2303967.
125 D. R. Larson, W. R. Zipfel, R. M. Williams, S. W. Clark, M. P. Bruchez, F. W. Wise and W. W. Webb, *Science*, 2003, **300**, 1434–1436.
126 J. Wu, N. Ji and K. K. Tsia, *Nat. Photonics*, 2021, **15**, 800–812.
127 A. Soleimany, D. K. Aghmiouni, M. Amirikhah, M. A. Shokrgozar, S. Khoee and B. Sarmento, *Adv. Funct. Mater.*, 2024, 202408594.
128 D. Kim, J. Kang, T. Wang, H. G. Ryu, J. M. Zuidema, J. Joo, M. Kim, Y. Huh, J. Jung, K. H. Ahn, K. H. Kim and M. J. Sailor, *Adv. Mater.*, 2017, **29**, 1703309.
129 G. Ramakrishna, O. Varnavski, J. Kim, D. Lee and T. Goodson, *J. Am. Chem. Soc.*, 2008, **130**, 5032–5033.
130 O. Varnavski, G. Ramakrishna, J. Kim, D. Lee and T. Goodson, *J. Am. Chem. Soc.*, 2010, **132**, 16–17.
131 P. Pan, L. Liu, L. Zhang, X. Wei, Y. Tian, X. Kang, Q. Zhang and M. Zhu, *Angew. Chem., Int. Ed.*, 2022, **61**, e202213016.
132 M. Zhu, C. M. Aikens, F. J. Hollander, G. C. Schatz and R. Jin, *J. Am. Chem. Soc.*, 2008, **130**, 5883–5885.
133 R. Philip, G. R. Kumar, N. Sandhyarani and T. Pradeep, *Phys. Rev. B: Condens. Matter Mater. Phys.*, 2000, **62**, 13160–13166.
134 V. Bonačić-Koutecký and R. Antoine, *Nanoscale*, 2019, **11**, 12436–12448.
135 R. Fathima and A. Mujeeb, *J. Alloys Compd.*, 2021, **858**, 157667.
136 J. Olesiak-Banska, M. Waszkielewicz, P. Obstarczyka and M. Samoc, *Chem. Soc. Rev.*, 2019, **48**, 4087–4117.
137 S. Knoppe, M. Vanbel, S. van Cleuvenbergen, L. Vanpraet, T. Bürgi and T. Verbiest, *J. Phys. Chem. C*, 2015, **119**, 6221–6226.
138 D. Arima, S. Hidaka, S. Yokomori, Y. Niihori, Y. Negishi, R. Oyaizu, T. Yoshinami, K. Kobayashi and M. Mitsui, *J. Am. Chem. Soc.*, 2024, **146**, 16630–16638.
139 X. Wang, B. Yin, L. Jiang, C. Yang, Y. Liu, G. Zou, S. Chen and M. Zhu, *Science*, 2023, **381**, 784–790.
140 S. Basu, M. P. Bakulić, Ž. S. Maršić, V. Bonačić-Koutecký and N. Amdursky, *ACS Nano*, 2023, **17**, 16644–16655.
141 J.-Y. Wang, J.-W. Yuan, X.-M. Liu, Y.-J. Liu, F. Bai, X.-Y. Dong and S.-Q. Zang, *Aggregate*, 2024, **5**, e508.
142 A. Ghosh, O. F. Mohammed and O. M. Bakr, *Acc. Chem. Res.*, 2018, **51**, 3094–3103.
143 G. Soldan, M. A. Aljuhani, M. S. Bootharaju, L. G. AbdulHalim, M. R. Parida, A.-H. Emwas, O. F. Mohammed and O. M. Bakr, *Angew. Chem., Int. Ed.*, 2016, **55**, 5749–5753.
144 M. van der Linden, A. J. van Bunningen, L. Amidani, M. Bransen, H. Elnaggar, P. Glatzel, A. Meijerink and F. M. F. de Groot, *ACS Nano*, 2018, **12**, 12751–12760.
145 W. Suzuki, R. Takahata, Y. Chiga, S. Kikkawa, S. Yamazoe, Y. Mizuhata, N. Tokitoh and T. Teranishi, *J. Am. Chem. Soc.*, 2022, **144**, 12310–12320.
146 N. Yan, N. Xia and Z. Wu, *Small*, 2021, **17**, 2000609.
147 S. Yang, J. Chai, Y. Song, J. Fan, T. Chen, S. Wang, H. Yu, X. Li and M. Zhu, *J. Am. Chem. Soc.*, 2017, **139**, 5668–5671.
148 J.-J. Fang, Z. Liu, Z.-Y. Wang, Y.-P. Xie and X. Lu, *Angew. Chem., Int. Ed.*, 2024, **63**, e202401206.
149 M. S. Bootharaju, H. Chang, G. Deng, S. Malola, W. Baek, H. Häkkinen, N. Zheng and T. Hyeon, *J. Am. Chem. Soc.*, 2019, **141**, 8422–8425.
150 D. Li, Z. Chen and X. Mei, *Adv. Colloid Interface Sci.*, 2017, **250**, 25–39.
151 Y. Zhou, W. Gu, R. Wang, W. Zhu, Z. Hu, W. Fei, S. Zhuang, J. Li, H. Deng, N. Xia, J. He and Z. Wu, *Nano Lett.*, 2024, **24**, 2226–2233.
152 X. Kang, S. Wang, Y. Song, S. Jin, G. Sun, H. Yu and M. Zhu, *Angew. Chem., Int. Ed.*, 2016, **55**, 3611–3614.
153 J. Zhou, X. Yang, P. Zheng, Q. Li, X. Li, J. Chai, B. Huang, S. Yang and M. Zhu, *Chem. Sci.*, 2024, **15**, 4853–4859.
154 C. Zhang, W.-D. Si, Z. Wang, C.-H. Tung and D. Sun, *Angew. Chem., Int. Ed.*, 2024, **63**, e202404545.
155 J. Lu, B. Shao, R.-W. Huang, L. Gutiérrez-Arzaluz, S. Chen, Z. Han, J. Yin, H. Zhu, S. Dayneko, M. N. Hedhili, X. Song, P. Yuan, C. Dong, R. Zhou, M. I. Saidaminov, S.-Q. Zang, O. F. Mohammed and O. M. Bakr, *J. Am. Chem. Soc.*, 2024, **146**, 4144–4152.
156 Z. Liu, M. Zhou, L. Luo, Y. Wang, E. Kahng and R. Jin, *J. Am. Chem. Soc.*, 2023, **145**, 19969–19981.
157 A. Pniakowska, K. K. Ramankutty, P. Obstarczyk, M. P. Bakulić, Ž. S. Maršić, V. Bonačić-Koutecký, T. Bürgi

and J. Olesiak-Bańska, *Angew. Chem., Int. Ed.*, 2022, **61**, e202209645.
158 Y. Zeng, S. Havenridge, M. Gharib, A. Baksi, K. L. D. M. Weerawardene, A. R. Ziefuß, C. Strelow, C. Rehbock, A. Mews, S. Barcikowski, M. M. Kappes, W. J. Parak, C. M. Aikens and I. Chakraborty, *J. Am. Chem. Soc.*, 2021, **143**, 9405–9414.
159 S. Kolay, S. Chakraborty, S. Pramanik and A. Patra, *J. Phys. Chem. C*, 2024, **128**, 7643–7651.
160 Z. Liu, Y. Li, W. Shin and R. Jin, *J. Phys. Chem. Lett.*, 2021, **12**, 1690–1695.
161 S. Kolay, S. Maity, S. Chakraborty, S. Ghosh and A. Patra, *J. Phys. Chem. C*, 2023, **127**, 3769–3777.
162 C. Yi, H. Zheng, L. M. Howard, C. J. Ackerson and K. L. Knappenberger Jr., *J. Phys. Chem. C*, 2015, **119**, 6307–6313.
163 S. Maity, S. Kolay, S. Ghosh, S. Chakraborty, D. Bain and A. Patra, *J. Phys. Chem. Lett.*, 2022, **13**, 5581–5588.
164 W.-Q. Shi, L. Zeng, R.-L. He, X.-S. Han, Z.-J. Guan, M. Zhou and Q.-M. Wang, *Science*, 2024, **383**, 326–330.
165 Y. Wang, Z. Liu, A. Mazumder, C. G. Gianopoulos, K. Kirschbaum, L. A. Peteanu and R. Jin, *J. Am. Chem. Soc.*, 2023, **145**, 26328–26338.
166 C. Yao, C. Q. Xu, I.-H. Park, M. Zhao, Z. Zhu, J. Li, X. Hai, H. Fang, Y. Zhang, G. Macam, J. Teng, L. Li, Q.-H. Xu, F.-C. Chuang, J. Lu, C. Su, J. Li and J. Lu, *Angew. Chem., Int. Ed.*, 2020, **59**, 8270–8276.
167 J.-Y. Wang, Y.-K. Li, X. Jing, P. Luo, X.-Y. Dong and S.-Q. Zang, *ACS Mater. Lett.*, 2022, **4**, 960–966.
168 H. Zheng, Y. Zhou, B. Yan, G. Zhou, X. Cheng, S. Lin, M. Duan, J. Li, L. Wang, C. Fan, J. Chen and J. Shen, *J. Am. Chem. Soc.*, 2024, **146**, 17094–17102.
169 L. Yang, H. Wang, D. Li, L. Li, X. Lou and H. Liu, *Chem. Mater.*, 2018, **30**, 5507–55155.
170 Y. Zhong, J. Zhang, T. Li, W. Xu, Q. Yao, M. Lu, X. Bai, Z. Wu, J. Xie and Y. Zhang, *Nat. Commun.*, 2023, **14**, 658.
171 H. Ma, X. Zhang, L. Liu, Y. Huang, S. Sun, K. Chen, Q. Xin, P. Liu, Y. Yan, Y. Wang, Y. Li, H. Liu, R. Zhao, K. Tan, X. Chen, X. Yuan, Y. Li, Y. Liu, H. Dai, C. Liu, H. Wang and X.-D. Zhang, *Sci. Adv.*, 2023, **9**, eadh7828.
172 C. Dai, C. Yang and X. Yan, *Nano Res.*, 2018, **11**, 2488–2497.
173 M. Shamsipur, E. Babaee, M.-B. Gholivand, F. Molaabasi, B. Hajipour-Verdom and M. Sedghi, *Biosens. Bioelectron.*, 2024, **250**, 116064.
174 S. He, H. Xiang, G. Zhao, M. Zhang, J. Lin, L. Yang and H. Liu, *Sens. Actuators, B*, 2023, **378**, 133182.
175 Y. Sun, Y. Zhang and Z. Wang, *Sens. Actuators, B*, 2021, **347**, 130661.
176 W. Wang, Y. Kong, J. Jiang, Q. Xie, Y. Huang, G. Li, D. Wu, H. Zheng, M. Gao, S. Xu, Y. Pan, W. Li, R. Ma, M. X. Wu, X. Li, H. Zuilhof, X. Cai and R. Li, *Angew. Chem., Int. Ed.*, 2020, **59**, 22431–22435.
177 A. Yahia-Ammar, D. Sierra, F. Mérola, N. Hildebrandt and X. Le Guével, *ACS Nano*, 2016, **10**, 2591–2599.
178 G. Yang, X. Pan, W. Feng, Q. Yao, F. Jiang, F. Du, X. Zhou, J. Xie and X. Yuan, *ACS Nano*, 2023, **17**, 15605–15614.
179 D. Li, Q. Liu, Q. Qi, H. Shi, E.-C. Hsu, W. Chen, W. Yuan, Y. Wu, S. Lin, Y. Zeng, Z. Xiao, L. Xu, Y. Zhang, T. Stoyanova, W. Jia and Z. Cheng, *Small*, 2020, **16**, 2003851.
180 G. Yang, K. Liu, Y. Wang, X. Pan, J. Ye, Y. Li, F. Du, T. Feng and X. Yuan, *Aggregate*, 2024, **5**, e435.
181 Rashi, V. Kaur, A. Devi, D. Bain, T. Sen and A. Patra, *J. Phys. Chem. Lett.*, 2023, **14**, 10166–10172.
182 A. Yadav, N. C. Verma, C. Rao, P. M. Mishra, A. Jaiswal and C. K. Nandi, *J. Phys. Chem. Lett.*, 2020, **11**, 5741–5748.
183 Z. Zhang, C. Liu, Y. Lu, W. Zhao, Q. Zhu, H. He, Z. Chen and W. Wu, *J. Nanobiotechnol.*, 2024, **22**, 488.
184 Y. Chen, M. L. Phipps, J. H. Werner, S. Chakraborty and J. S. Martinez, *Acc. Chem. Res.*, 2018, **51**, 2756–2763.
185 R. Nagda, S. Park, I. L. Jung, K. Nam, H. C. Yadavalli, Y. M. Kim, K. Yang, J. Kang, P. W. Thulstrup, M. J. Bjerrum, M. Cho, T.-H. Kim, Y. H. Roh, P. Shah and S. W. Yang, *ACS Nano*, 2022, **16**, 13211–13222.
186 Z. Lin, N. Goswami, T. Xue, O. J. H. Chai, H. Xu, Y. Liu, Y. Su and J. Xie, *Adv. Funct. Mater.*, 2021, **31**, 2105662.
187 Q. Zhuang, H. Jia, L. Du, Y. Li, Z. Chen, S. Huang and Y. Liu, *Biosens. Bioelectron.*, 2014, **55**, 76–82.
188 E. A. Halabi and R. Weissleder, *J. Am. Chem. Soc.*, 2023, **145**, 8455–8463.
189 B. Lozano-Torres, I. Galiana, M. Rovira, E. Garrido, S. Chaib, A. Bernardos, D. Muñoz-Espín, M. Serrano, R. Martínez-Máñez and F. Sancenón, *J. Am. Chem. Soc.*, 2017, **139**, 8808–8811.